iScience

CellPress
REVIEWS

Review

Surfactant-Assisted Cooperative Self-Assembly of Nanoparticles into Active Nanostructures

Wenbo Wei,[1] Feng Bai,[1,*] and Hongyou Fan[2,3,4,*]

Nanoparticles (NPs) of controlled size, shape, and composition are important building blocks for the next generation of devices. There are numerous recent examples of organizing uniformly sized NPs into ordered arrays or superstructures in processes such as solvent evaporation, heterogeneous solution assembly, Langmuir-Blodgett receptor-ligand interactions, and layer-by-layer assembly. This review summarizes recent progress in the development of surfactant-assisted cooperative self-assembly method using amphiphilic surfactants and NPs to synthesize new classes of highly ordered active nanostructures. Driven by cooperative interparticle interactions, surfactant-assisted NP nucleation and growth results in optically and electrically active nanomaterials with hierarchical structure and function. How the approach works with nanoscale materials of different dimensions into active nanostructures is discussed in details. Some applications of these self-assembled nanostructures in the areas of nanoelectronics, photocatalysis, and biomedicine are highlighted. Finally, we conclude with the current research progress and perspectives on the challenges and some future directions.

INTRODUCTION

Nanoparticles (NPs) of controlled size, shape, and composition are important building blocks within the nanoscience and engineering communities (Gong et al., 2017). Organizing NPs into highly ordered arrays, or the so-called "metamaterials," which exhibit collective electronic, magnetic, and optical behaviors, enables their great potential for nanoelectronic and nanophotonic applications (Bian et al., 2018; Ortega et al., 2017; Kovalenko et al., 2015; Boles et al., 2016; Yin and Alivisatos, 2004; Sun, 2013; Gilroy et al., 2016; Tao et al., 2008). There are numerous recent examples of organizing uniformly sized NPs into ordered arrays or superstructures in processes such as solvent evaporation, solution growth, Langmuir-Blodgett receptor-ligand interactions, and layer-by-layer assembly (Boles et al., 2016; Kotov et al., 1995; Lu and Tang, 2016; Lai et al., 2016; Tao et al., 2008; Zhang et al., 2013; Hong et al., 2017). NPs are stabilized through surface functionalization with organic ligands or active surfaces. These ligands protect the NPs from aggregation on the one hand and render the driving forces for self-assembly and formation of NP superstructures on the other hand. To date, most previous works focus on the NPs functionalized with alkane chains as the ligand (Kovalenko et al., 2015). The nature of alkane chains causes the resultant NPs to be hydrophobic and to dissolve only in organic solvents (e.g., toluene). As such, methods such as solvent evaporation, solution growth, and Langmuir-Blodgett have been explored to form highly ordered well-defined NP nanostructures through balanced interparticle interactions, such as hydrophobic-hydrophobic interactions, repulsion, and dipolar interactions. Methods such as solvent evaporation and solution growth lead to 3D superlattice or supercrystals, whereas uniform 2D monolayer of NP arrays can be formed by using the Langmuir-Blodgett approach. Besides these alkane-chain-functionalized hydrophobic NPs, other NP active surfaces such as DNA biofunctionalization have been explored (Tian et al., 2016; Hong et al., 2017). One can use DNA as molecular scaffolds to control NP self-assembly to form hierarchical NP nanostructures that resemble DNA scaffolds (Liu et al., 2016; Hong et al., 2017). Overall, these self-assembled NP nanostructures provide well-defined systems for studies of NP coupling and interactions for optoelectronic applications. In recent reviews, these progresses have been very well documented (Grzelczak et al., 2010; Lu and Yin, 2012; Wang et al., 2013a; Vogel et al., 2015).

In this review, we summarize the recent advances on the surfactant-assisted cooperative self-assembly of NPs using amphiphilic surfactants and NPs to synthesize new classes of highly ordered active nanostructures. We start with a brief overview of the concept of the surfactant-assisted cooperative self-assembly. Then detailed discussions will be made on how the approach works with nanoscale materials of different dimensions, such as spherical NPs, 1D nanorods, and 2D nanosheets in active nanostructures. We highlight

[1]Key Laboratory for Special Functional Materials of Ministry of Education, National & Local Joint Engineering Research Center for High-efficiency Display and Lighting Technology, School of Materials Science and Engineering, Collaborative Innovation Center of Nano Functional Materials and Applications, Henan University, Kaifeng 475004, China

[2]Department of Chemical and Biological Engineering, The University of New Mexico, Albuquerque, NM 87131, USA

[3]Advanced Materials Laboratory, Sandia National Laboratories, Albuquerque, NM 87106, USA

[4]Center for Integrated Nanotechnologies, Sandia National Laboratories, Albuquerque, NM 87185, USA

*Correspondence: baifengsun@126.com (F.B.), hfan@sandia.gov (H.F.)

https://doi.org/10.1016/j.isci.2018.12.025

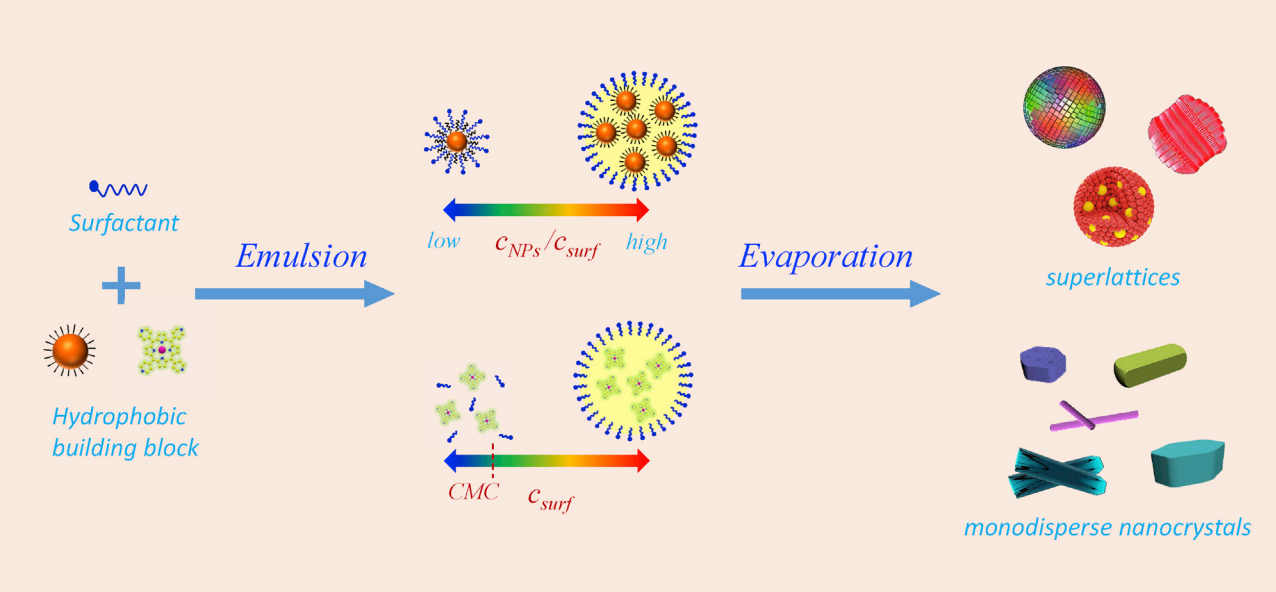

Figure 1. Schematic Illustration for the Surfactant-Assisted Cooperative Self-Assembly

some promising applications of these self-assembled nanostructures in the areas of nanoelectronics, photocatalysis, and biomedicine. Finally, we conclude with the current research progress and our perspectives on the challenges and some future directions.

Surfactant-Assisted Cooperative Self-Assembly

Surfactant-assisted cooperative self-assembly achieves well-defined active nanomaterial structures and properties by confining the NP self-assembly or growth within nanocompartments—such as micelles, emulsions, and mesophases—formed by amphiphilic surfactants in aqueous solutions (Figure 1) (Fan et al., 2004). Surfactants are amphiphilic molecules that have hydrophilic groups (heads) and hydrophobic groups (tails). In aqueous solutions, they form aggregates, such as micelles, which are tiny (5–50 nm) structures with a hydrophilic exterior and a hydrophobic interior. In simple terms, the hydrophilic heads link up in an aqueous solution to create a spherical shell that encapsulates the hydrophobic tails away from the solution. Hydrophobic NPs or precursors can be encapsulated within the hydrophobic micellar interiors, as typically happens with hydrophobic NPs or oil-like species. As noted above, other surfactant aggregates such as mesophases can also form depending on the concentration and types of surfactants. Growth from NPs to seed structures and then to final highly ordered superstructures through cooperative interactions between NPs is confined within the micelles (or other surfactant aggregates), giving rise to uniform and complex 1D–3D NP active nanostructures.

Key factors that control the self-assembly processes are summarized in Table 1. First, the building blocks need to be hydrophobic for encapsulation inside the micelles. Second, heating is required to remove the oil phase or organic solvents from the emulsions to initiate the self-assembly process. The temperature should be higher than the boiling point of the oil or solvents and lower than that of water. Higher temperatures (more than 70°C) are usually used to prepare ordered superparticles, because the thermal energy facilitated adjustment of the spatial position of the NPs and counteracted the loss of the configurational entropy. Otherwise, when the temperature was decreased to 40°C, random superparticles were obtained because the thermal energy was not sufficient to overcome the loss of configurational entropy. Third, the self-assembly process critically relies on the surfactant concentrations. The surfactant concentrations should be equal to the critical micelle concentration or higher to induce the formation of NP-micelles. Depending on the surfactant concentration, surfactant mesophases can be formed for complex NP superstructures. Finally, as the final nanostructures relied on the interdigitation between the organic ligands and surfactant hydrophobic tail groups, alkane chains of surfactants and organic ligands with a minimum of 8–10 carbons are desirable to stabilize NP-micelles and other NP superstructures.

Temperature	Higher than the boiling point of organic solvents, lower than that of water
Surfactant concentration	1) Higher than CMC for NP-micelles 2) High concentration favorable for mesophase for superstructure formation
Surfactant size	Alkane chains larger than 8 carbon

Table 1. Key Factors That Control the Self-Assembly Process

Formation of NP-Micelles

NPs have demonstrated important biomedical applications such as bioimaging and biosensing (Nam et al., 2013; Li et al., 2017). These applications require them to be water soluble and biocompatible in biological environments. Most of the organically passivated NPs have hydrophobic surface chemistry making them unsuitable for direct bioapplications, whereas surfactant-assisted self-assembly can effectively functionalize NPs to form NP-micelles that are water soluble and biocompatible. By surfactant-assisted self-assembly, organically passivated hydrophobic NPs could be transferred to aqueous phase forming NP-micelles (Fan, 2008; Fan et al., 2004, 2005b). The NP-micelles are composed of NPs at the core and a hybrid bilayer shell that is formed by interdigitated alkane chains from the organic ligands (the primary layer) on NP surface and the surfactants (the secondary layer) (Figure 1). The interdigitation of the alkane chains is thermodynamically favorable to lock in the bilayer structure, which renders the NP-micelle stable in aqueous solutions. The thicknesses of the bilayer could be precisely defined by primary and secondary layers (Fan et al., 2005b). Depending on the length of the alkane chains, surfactants and organic ligands with a minimum of 8–10 carbons are desirable to stabilize the NP-micelles (Fan et al., 2004). The surfactant-assisted cooperative assembly method can be extended effectively to prepare water soluble and biocompatible semiconductor and magnetic NP-micelles for *in vitro* and *in vivo* imaging and drug delivery (Liong et al., 2008, 2009a; Kim et al., 2006, 2008).

Semiconductor NPs or quantum dots (QDs) are fluorescent nanocrystals (NCs) that provide distinct advantages over conventional organic dyes or fluorescent proteins. The advantages include the large absorption coefficient, bright Photoluminescence (PL) emission (~10–100 times brighter than that of single organic dye), a narrow and symmetric emission profile, and high photochemical stability (Medintz et al., 2005). The high photostability and notable brightness of QDs can allow long-term acquisition of PL emissions with a good signal-to-noise ratio (Jaiswal et al., 2003). These unique properties provide a unique opportunity for cellular labeling and *in vivo* imaging (Mattoussi et al., 2012). As QDs are normally stabilized by organic alkane ligands and are therefore hydrophobic, they often need surface modifications to obtain biocompatibility. Encapsulation of QDs in micelles of lipids or surfactants to form QD-micelles through surfactant-assisted cooperative assembly can effectively preserve the optical properties of as-synthesized QDs while providing biocompatibility (Fan et al., 2005b).

For preparing biocompatible QD-micelles, monodisperse CdSe and CdSe/CdS core/shell QDs were used as the fluorescent core of the QD-micelles (Fan et al., 2005b; Dubertret et al., 2002). A concentrated suspension of QDs in chloroform was added to an aqueous solution containing a mixture of surfactants or phospholipids with different functional head groups, such as ethylene glycol (–PEG, [polyethylene glycol]) and amine (–NH_2). The –PEG group was used to improve biocompatibility, and the -NH_2 amine group provided sites for further bioconjugation. Because the surfactant-assisted self-assembly does not chemically change the nature of the QDs, the QD-micelles essentially preserve their optical property from the original hydrophobic QDs. For example, the acquired QD-micelle solutions exhibited the same visible and emission colors as their hydrophobic counterparts, as shown in the optical micrograph (Figure 2A). Optical spectra, including ultraviolet-visible (UV-vis) spectroscopy (Figure 2B) and PL (Figure 2D), further confirm the preservation of the optical property of the original QDs after formation of QD-micelles. Besides the optical property, the QD-micelles also maintain the structural monodispersity of the original QDs. Transmission electron microscopic images show the formation of ordered hexagonal close packing of QD-micelles (Figure 2C), as expected for individual monosized QDs. Studies of photostability of the water-soluble QD-micelles under long-time laser irradiation showed that these NC-micelles exhibited no loss of PL intensity in water. Because of the interdigitated phospholipid bilayer interface at the QD-micelle surface, the QD-micelles exhibit very good biocompatibility, which was evaluated by examination of

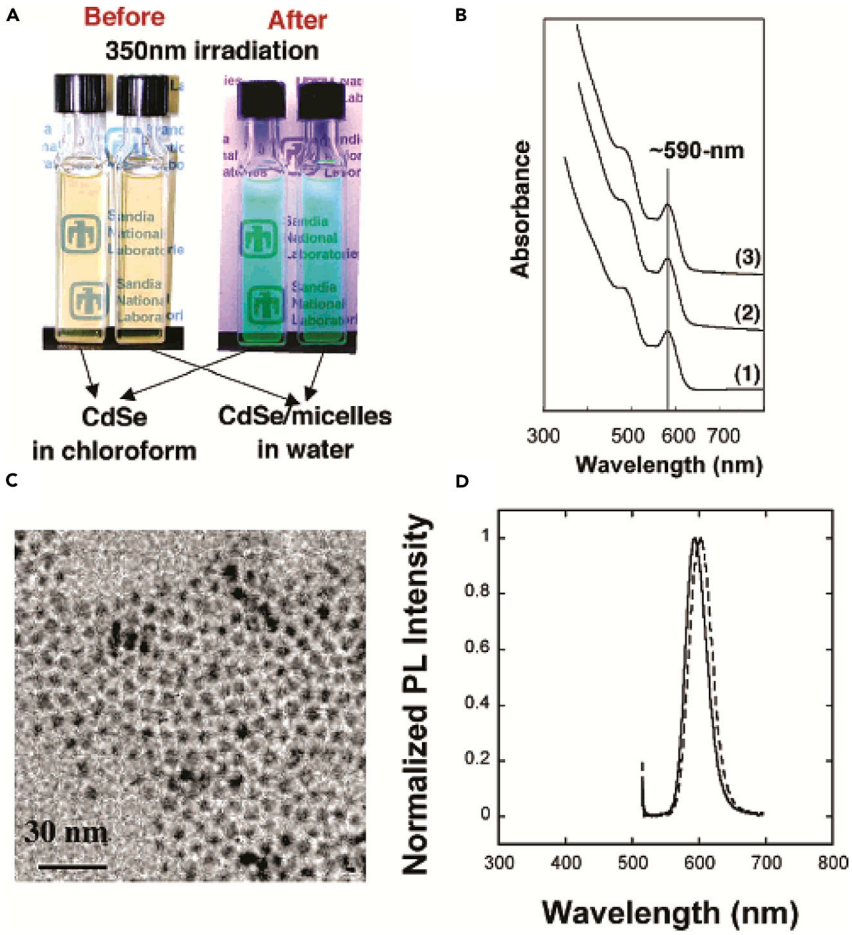

Figure 2. Biocompatibility of QD-Micelles

(A) An optical micrograph of CdSe QDs in chloroform and CdSe-micelles in water prepared using cetyl trimethylammonium bromide.

(B) UV-vis spectra of (1) CdSe/CdS in hexane, (2) CdSe/CdS QD-micelles prepared using 1,2-dioctanoyl-sn-glycero-3-phosphocholine (C8-lipid) and hexadecylamine, and (3) 1,2-distearoyl-sn-glycero-3-phosphoethanolamine-N-amino (polyethylene glycol) and dipalmitoyl phosphatidylcholine.

(C) Transmission electron microscopic image of CdSe/CdS QD-micelles.

(D) PL of CdSe/CdS in toluene (solid line) and C8-lipid-encapsulated CdSe/CdS QD-micelles in water (dashed line).

Reprinted with permission from Fan et al. (Fan et al., 2005b). Copyright 2005 American Chemical Society.

their uptake in cultured rat hippocampal neurons and other bioenvironments (Fan et al., 2005b; Lidke et al., 2004; Dubertret et al., 2002). The retained fluorescence character after a fairly long incubation suggested the effective biocompatibility of the QD-micelles (Jaiswal et al., 2003).

Besides semiconductor QDs, magnetic NPs have also been functionalized for bioapplications based on surfactant-assisted self-assembly. For example, Kim and co-workers use this approach to prepare discrete, monodisperse, and size-controllable core-shell mesoporous silica NPs by using Fe_3O_4 nanocrystals as the core for simultaneous magnetic resonance (MR) and fluorescence imaging, and for drug delivery (Kim et al., 2006, 2008). In their procedure, cetyl trimethylammonium bromide (CTAB) serves both as the stabilizing surfactant for transferring hydrophobic Fe_3O_4 NPs to aqueous phase and as the organic template for the formation of mesopores in the sol-gel reaction. The surface of the NPs was modified with PEG to render them biocompatible by preventing the nonspecific adsorption of proteins to the NPs. The acquired Fe_3O_4@mSiO_2 particles are monodisperse and with diameters ranging from 45–105 nm. Worm-like mesopores with diameters of around 2–3 nm were observed in the silica shells and provide the potential ability for drug delivery. The products maintained the superparamagnetic property characterized by

field-dependent magnetization at room temperature, which is a desirable characteristic for MR contrast agents (Lee and Hyeon, 2012). The NPs can be spontaneously internalized into MCF-7 cells by endocytosis, and their uptake was clearly observed within 30 min. The core-shell nanostructures were also maintained after endocytosis. NPs with different compositions and shapes such as MnO and silver NPs have been demonstrated for preparing biocompatible NP-micelles for applications as MR imaging contrast agent or antimicrobial agents, respectively (Na et al., 2007; Liong et al., 2009b). In addition, $FeMnO_4$ and FePt NP-micelles have been prepared by using surfactant-assisted self-assembly (Fan et al., 2005a).

In addition to bioapplications, NP-micelles have been demonstrated to be a functional building block for further self-assembly into robust, highly ordered NP arrays for nanoelectronic or nanophotonic devices (Fan et al., 2006). Because of the interdigitated surfactant bilayer structure, the NP-micelle surface affords flexible surface chemistry and active function depending on the use of different surfactants. Using the NP-micelles as a building block, formation of 2D ordered NP arrays and 3D NP superlattices by the evaporation-induced self-assembly process have been demonstrated. For example, drying of a gold NP-micelle solution on solid substrates can result in hexagonal close-packed 2D superlattices. If a concentrated NP-micelle aqueous solution is used for directly drying, 3D superlattices with face-centered cubic (fcc) symmetry can be formed. The robustness of this approach allows tuning of interparticle spacing through the use of various space molecules (Fan et al., 2005a).

Through a hydrothermal sol-gel self-assembly process, the NP-micelles self-assembled with silica into hierarchically ordered composite mesophase crystals (Wright et al., 2006). The process involved two steps: (1) preparation of an NP-micelle solution through surfactant-assisted cooperative self-assembly process and (2) hydrothermal nucleation and growth of mesophase crystals using NP-micelles. Through the hydrothermal self-assembly process, well-shaped and oriented NP/silsesquioxane crystals were formed on substrates over several hours. These crystals were fairly uniform in shape and size with flower-like hierarchical structure and the NP-micelles self-assembled as an fcc mesophase inside these crystals.

Through the sol-gel process, the NP-micelles have been used to form thin films of ordered gold NP silica arrays (Fan et al., 2004). By suppressing siloxane condensation and thereby gel formation, solvent evaporation induced self-assembly of gold NP-micelles with silica into a thin film. The final film consists of monodisperse gold NPs arranged within silica or organosilsesquioxane host matrices in an fcc mesostructure with precisely controlled interparticle spacing. The gold NP/silica composite films are transparent when less than 300 nm thick and have an average refractive index of ~1.7. The film thickness can be controlled from 100 nm to several micrometers.

Overall, the surfactant-assisted cooperative self-assembly method provides several advantageous features to synthesize solid NP arrays for practical applications. First, self-assembly of NP-micelles allows for the preparation of ordered NP arrays in aqueous phase, resulting in enhanced safety and better compatibility with current semiconductor fabrication and integration processes. Second, this method allows simple tuning of framework composition, and thus dielectrics, between NPs. This is essential to achieve enhanced transport properties of such three-dimensional superlattice films. Finally, the formation of self-assembled NP solids in inorganic matrix through cooperative self-assembly of NP-micelles and inorganic precursors (e.g., silica) essentially improves NP thermal stability for enhanced practical applications.

Another route that utilizes surfactant-assisted self-assembly for the synthesis of 3D self-assembled nanostructure was reported by Cao group (Figure 3) (Zhuang et al., 2007, 2008). They used oleic-acid-functionalized Fe_3O_4 nanocrystals as core and dodecyl trimethylammonium bromide (DTAB) as the surfactant to make NP-micelles. When injecting the NP-micelle solution into a polyvinylpyrrolidone (PVP) ethylene glycol solution, DTAB molecules were detached into the ethylene glycol solution due to a decrease of van der Waals interactions between nanocrystal ligands and surfactants (DTAB), causing the NP-micelles to decompose. As a result, solvophobic interactions between nanocrystal surface ligands and ethylene glycol/water solvent molecules were induced, leading to nanocrystal aggregation and the formation of superparticles. The superparticle formation is a very rapid process that takes only 1 min, implying that it is a kinetically controlled process.

The formation of NP-micelles represents a new synthetic methodology for functionalizing NPs, enabling flexible NP surface chemistry and function. The method is easy, rapid, and universal for preparing water-soluble, biocompatible and size-controllable nanomaterials for bioimaging and drug delivery applications.

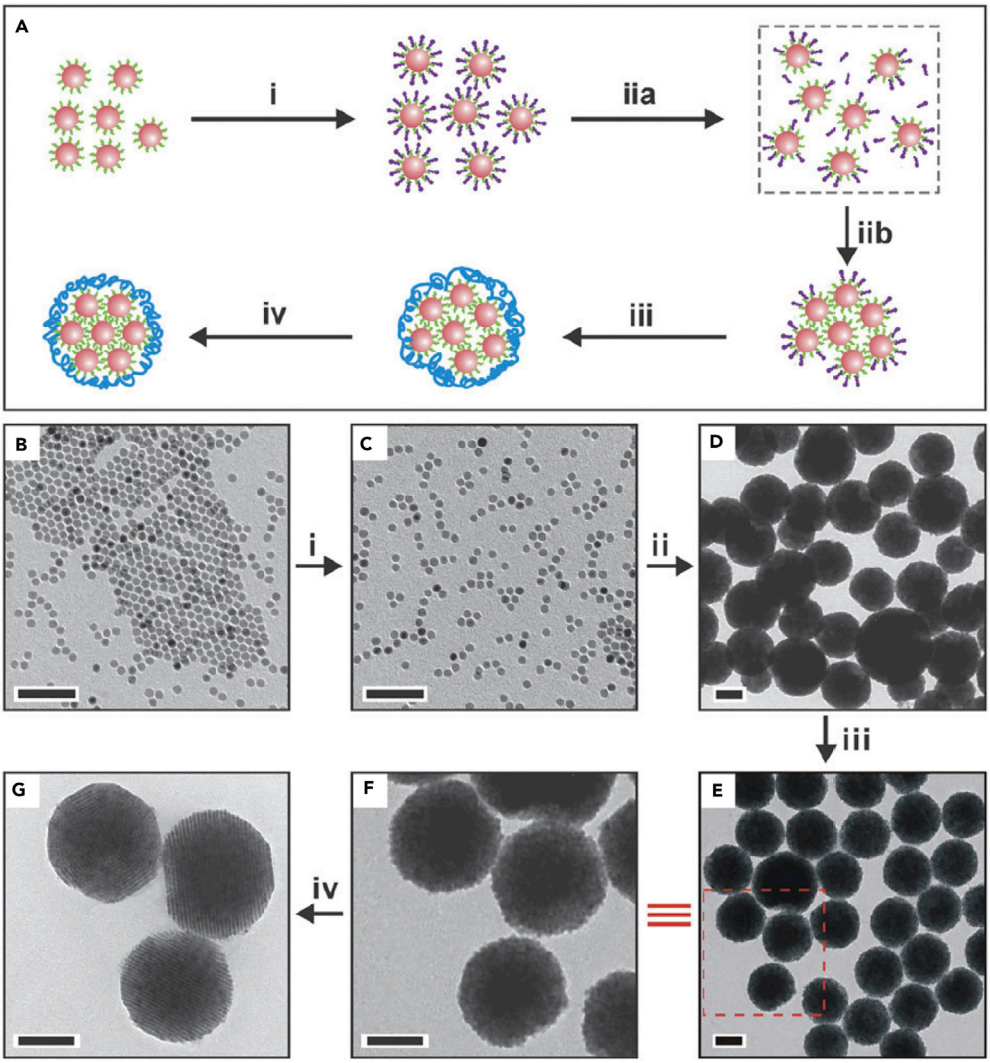

Figure 3. Surfactant-Assisted Self-Assembly and Formation of 3D Superparticles

(A) Schematic representation of the proposed formation mechanism of 3D self-assembly superparticles.

(B) Transmission electron microscopic (TEM) image of oleic-acid-functionalized Fe_3O_4 nanocrystals.

(C) DTAB-Fe_3O_4 nanocrystal micelles.

(D) superparticles made without PVP. (E) superparticles capped with PVP. (F) An enlarged image of the inset in (E).

(G) superparticles after annealing at 80°C for 6 h.

Scale bars, 50 nm in (B and C) and 100 nm in (D–G). Reproduced with permission from Wang et al. (Wang et al., 2013a). Copyright 2013 of the Royal Society of Chemistry.

Emulsion-Confined Formation of 3D Superparticles

Colloidal NP superparticles are an important class of materials that are self-assembled from size- and shape-controlled NPs. The typical sizes of the superparticles are in the mesoscopic regime, ranging from tens of nanometers to a few micrometers. The superparticles exhibit not only intrinsic physical characteristics of their nanometer-sized particles but also collective properties of the self-assembled NPs due to coupling effects (Wang et al., 2013a). The properties of superparticles can be tuned by the size, shape, and composition of the initial NPs. These promises have stimulated extensive research efforts to study superparticle formation. Previous works were mainly focused on noncovalent interactions between hydrophobic NPs (Boles et al., 2016). Surfactant-assisted cooperative self-assembly relies on the formation of emulsions by increasing NP concentration (Bai et al., 2007). During the formation of NP-micelles, there are enough surfactants to encapsulate individual NPs to form interdigitated bilayers around individual NPs. If the NP concentration is increased in the self-assembly solutions, there is not a large enough amount

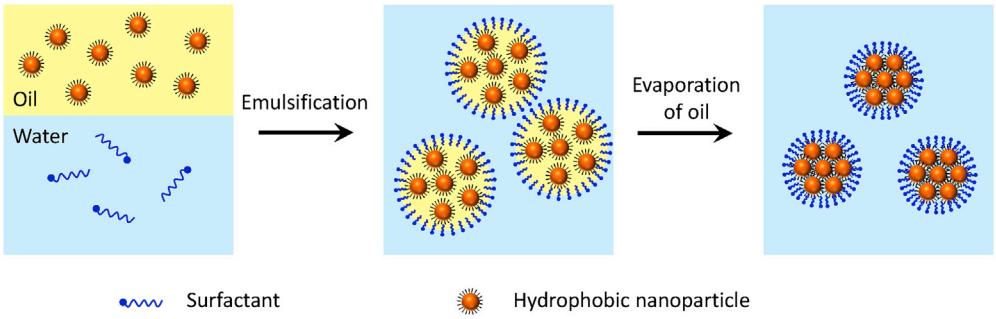

Figure 4. Emulsion-Confined Formation of 3D Superparticles

Bai et al. demonstrated formation of $BaCrO_4$ superparticles by using anionic surfactant sodium dodecyl sulfate (SDS) to create an oil-in-water microemulsion by ultrasonic treatment (Bai et al., 2007). Typical sizes of the assembled $BaCrO_4$ superparticles are in the range of 100–120 nm. One important feature is that the constituent NPs retain their individual physical characteristics and do not sinter into larger particles. This is likely due to the fact that the self-assembly process relies on noncovalent interactions without chemical changes of the NPs. The surfactant bilayer surface has proved to be critical in stabilizing the superparticle. The zeta potential was measured to be a negative surface charge with potential of −27.6 mV, which is consistent with the use of SDS. In another example, when positive-charge surfactant CTAB is used to prepare Ag_2Se superparticles, zeta potential characterizations indicate that these colloidal sphere assemblies have a positive charge with potential of +38.0 mV.

of surfactants to form interdigitated bilayers around individual NPs. Instead, microemulsions are formed with NPs in oil (or organic solvent) phase. Surfactants at the interface between the oil and aqueous phases of the microemulsions shield the NPs from the aqueous phase to form stable NP/solvent/water microemulsions. Thus NPs are confined within the microemulsion droplets. Subsequent self-assembly is initiated by evaporation of organic solvents through heating or vacuum. Evaporation of organic solvents progressively enriches the concentration of the NPs in microemulsion droplets, which induces the noncovalent interactions and self-assembly to produce superparticles (Figure 4). In this process, self-assembly is based on a subtle balance of entropy arguments and van der Waals attractions between NPs and the alkane chains of the ligands located on the NPs. The alkane chains of the surfactants from the aqueous phase spontaneously interdigitate with the alkane chains of the primary ligands located on the outside surface of the NP assemblies through hydrophobic-hydrophobic and van der Waals interactions. The resultant colloidal NP superparticles can be well dispersed in aqueous solution and can be collected and purified by centrifugation or filtration.

The above results show that this approach is a simple and facile synthetic method for preparing colloidal superparticles from NP building blocks. This method has been successfully demonstrated in a wide range of NPs, including $BaCrO_4$, Ag_2Se, CdS, PbS, Fe_3O_4, ZrO_2, $NaYF_4$, TiO_2, $CoFe_2O_4$, CeO_2, Bi_2S_3 nanoplates, $PbSeO_3$ nanorods, and LaF_3 nanoplates (Wang et al., 2018a; Lu et al., 2010; Bai et al., 2007; de Nijs et al., 2015; He et al., 2017b), as shown in Figure 5. The diameters of these superparticle spheres range from 50 to 200 nm, depending on the size of the microemulsion droplets formed for a given set of the designed experimental conditions. The diameter of the colloidal spheres can be controlled by adjusting the emulsification processes, NP concentrations in the oil phase, surfactant concentrations in the water phase, and oil-to-water ratio. A stronger emulsification process gives smaller emulsion droplets, and thus produces smaller superparticles (Bai et al., 2007). For example, CdS superparticles with a diameter larger than 500 nm were obtained by stirring (greater than 1,500 rpm), and superparticle spheres with a diameter less than 300 nm were obtained by strong sonication emulsification. In addition, higher NP concentrations in the oil phase result in a larger sphere diameter due to the increased NP numbers in the emulsion. Accordingly, decreasing the surfactant concentrations in the water phase or increasing the oil-to-water ratio results in larger emulsion droplets and thus increases the diameter of the products. It is interesting to note that extra amounts of surfactants in both the oil and water phases play an important role in stabilizing microemulsion droplets. In some cases when extra surfactants are used, hollow assembly structures can be obtained instead of solid superparticle spheres. For example, Park et al. prepared vesicle-like 2D assembled iron oxide nanostructures by adding extra sodium oleate (Park et al., 2016).

Temperature has been identified to be an important factor influencing the surfactant-assisted self-assembly because heating is needed to evaporate the organic solvents to induce NP self-assembly. Too

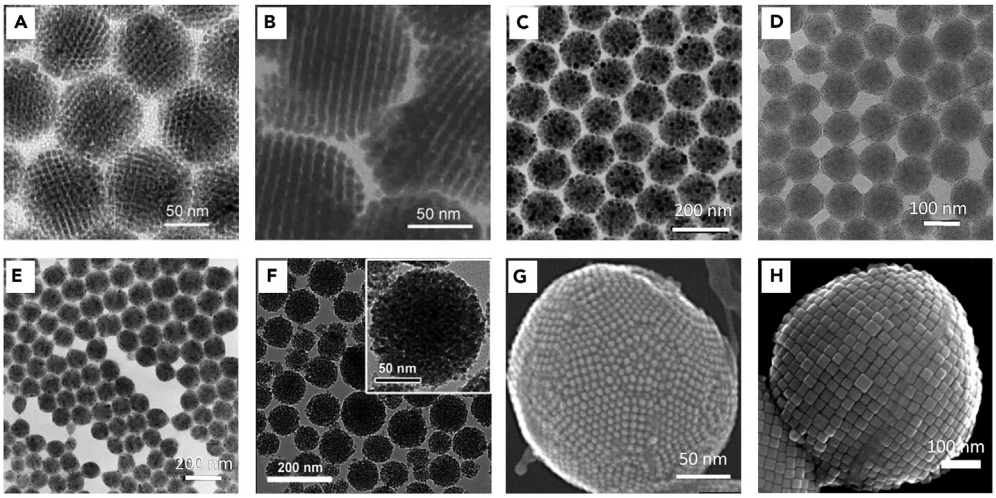

Figure 5. Colloidal Superparticles Self-Assembled from Different NPs

(A–E) (A) $BaCrO_4$, (B) Ag_2Se, (C) PbS, (D) ZrO_2, (E) $NaYF_4$. Reproduced with permission from Bai et al. (Bai et al., 2007). Copyright 2007 John Wiley & Sons, Inc.

(F) TiO_2. Reproduced with permission from Lu et al., 2010. Copyright 2010 John Wiley & Sons, Inc.

(G) $CoFe_2O_4$. Reproduced with permission from Nijs et al. (de Nijs et al., 2015). Copyright 2015 Macmillan Publishers Ltd.

(H) Fe_3O_4 nanocubes. Reproduced with permission from Wang et al. (Wang et al., 2018a). Copyright 2018 Macmillan Publishers Ltd.

high temperature could cause NP sinter and could chemically change the chemical and physical structures and properties of the NPs. In general, temperatures lower than 100°C are enough to remove most organic solvents, such as chloroform and toluene, without sintering the NPs. Depending on the boiling points of the solvents, solvents such as chloroform can be readily removed at room temperature. It is also noted that if the evaporation times are much longer than the self-assembly equilibration time of the colloidal systems, disordered assemblies (icosahedral colloidal clusters) can be formed (de Nijs et al., 2015).

Luo et al. reported 3D highly compacted superparticles that were fabricated through a thermally controlled emulsion-based self-assembly method (Figure 6) (Luo et al., 2017). They used CdSe QDs, DTAB, and chloroform to initiate the formation of oil-in-water emulsions. When evaporating at 70°C, ordered CdSe superparticles were formed. In this situation, the thermal energy facilitated adjustment of the spatial position of the NPs and counteracted the loss of the configurational entropy, which resulted in the formation of highly ordered superparticles. However, when the temperature was decreased to 40°C, random superparticles were obtained because the thermal energy was not sufficient to overcome the loss of configurational entropy. In addition, only monodispersed QD-DTAB micelles were obtained without an additional heat source (stay at 20°C). Because of the ordered structure, the NPs within the superparticles are highly compacted, which promotes coupling and electronic energy transfer between CdSe QDs. Therefore, the acquired QD superparticles exhibited different optical properties and enhanced photoelectric activity compared with the original QDs.

In another work, Park et al. reported the formation of self-assembled low-dimensional superparticles with hollow vesicle-like structures under low evaporation temperature (Figure 7) (Park et al., 2016). In the assembly, the emulsion was initiated with a chloroform solution of iron oxide NPs in an aqueous solution of CTAB under stirring. By evaporating chloroform from the emulsion overnight at 40°C, hollow vesicle-like NP structures were formed instead of solid superparticles. They found that oil-in-water pickering emulsion droplets were initially formed upon mixing the two phases, allowing the oil-water interfaces to be stabilized by both surfactants and NPs. As chloroform diffused out and was evaporated and water diffused in over time, the polarity of the core solvent increased and more NPs accumulated at the interface. Finally, NPs were trapped into a curved 2D membrane structure encasing water. When evaporating chloroform at a high temperature, the thermodynamically stable structure of compact spherical assemblies was formed. It is interesting to note that the relatively high solubility of chloroform in water (25°C, 0.82% w/w) also promotes the

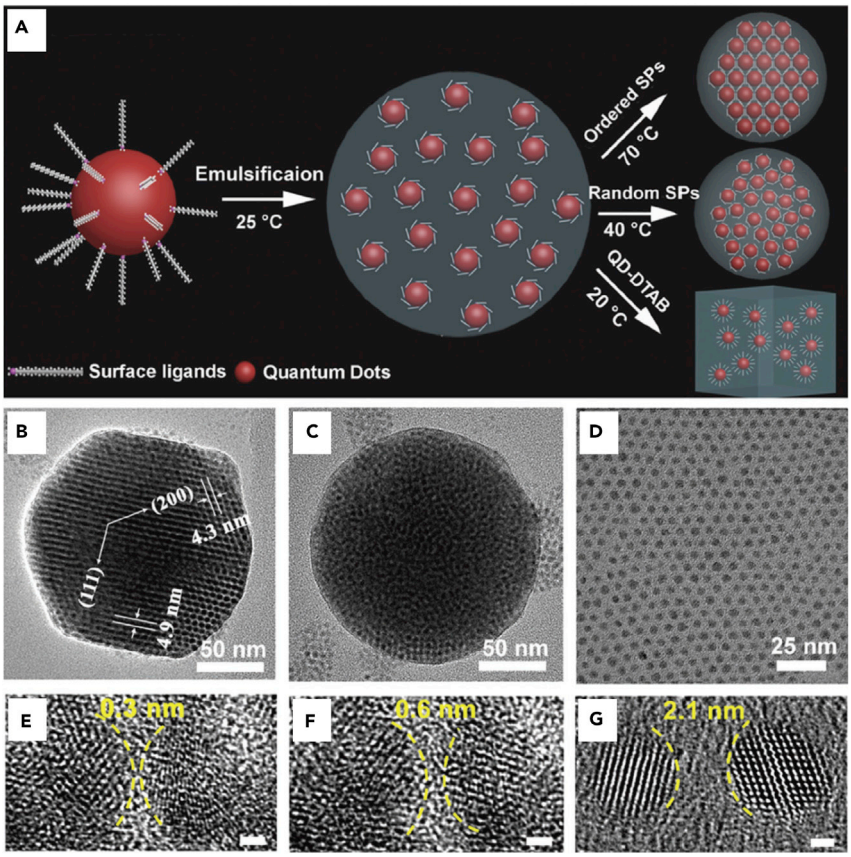

Figure 6. Temperature-Controlled Surfactant-Assisted Emulsion Self-Assembly

(A) Schematic representations of the thermally controlled, emulsion-based bottom-up self-assembly process.

(B–D) Low-magnification transmission electron microscopic (TEM) images of (B) an ordered superparticle exhibiting superlattice fringes of d(200) = 4.3 nm and d(111) = 4.9 nm, (C) a random superparticle, and (D) ordered arrays.

(E–G) High-magnification TEM images showing the distance between two neighboring QDs in (E) ordered superparticles, (F) random superparticles, and (G) ordered arrays (scale bar, 1 nm).

Reprinted with permission from Luo et al. (Luo et al., 2017). Copyright 2017 John Wiley & Sons, Inc.

formation of hollow assemblies, as it allows for the exchange of the two solvents while keeping the hollow structure intact.

In the above discussions, we have highlighted the superparticles that are formed from one type of NPs. Multicomponent NP nanostructures self-assembled from more than one type of NPs represent a new pathway for generating complex active superparticles with multiple functions for various technological applications (Suh et al., 2009; Bigall et al., 2012; Tan et al., 2016). These multicomponent NP nanostructures not only enhance the size-dependent properties of their individual components but also manifest novel interactions and synergistic properties from the near-field coupling that occurs between neighboring NPs.

Using the surfactant-assisted self-assembly process, Zhang et al. successfully prepared Au/CdSe superparticles that exhibit dual functions from both Au and CdSe (Shi et al., 2017). Au NPs of specific sizes (2.8, 4.6, 7.2, or 9.0 nm) and CdSe QDs of size 3.3 nm were assembled into large spherical superparticles of diameter ~100 nm. They controlled the spatial distribution of Au NPs and CdSe QDs in the assembly by changing the weight ratio of the two components. Energy-dispersive X-ray spectroscopy mapping showed a uniform distribution of Cd and Se over the whole cluster, with Au dispersed sporadically (Figure 8). Using finite-difference time-domain modeling, time-resolved PL spectra, and wavelength-dependent illumination tests, they presented strong evidence of an efficient plasmon resonance energy transfer from the Au NPs to the CdSe QDs, which enhances charge carrier generation in the semiconductor and suppresses bulk recombination.

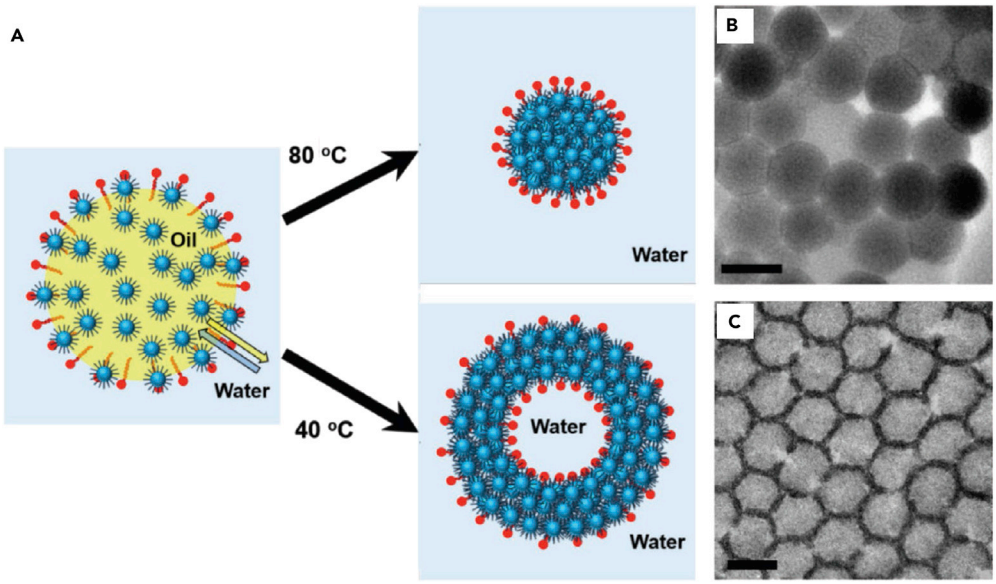

Figure 7. Surfactant-Assisted Self-Assembly and Formation of Solid and Hollow Superparticles
(A) Schematic description of iron oxide NP assemblies formed at two different temperatures.
(B) Transmission electron microscopic (TEM) images of solid superparticles.
(C) TEM images of hollow superparticles. Scale bars, 500 nm.
Reproduced with permission from Park et al. (Park et al., 2016). Copyright 2016 John Wiley & Sons, Inc.

The additional electron-hole pairs in adjacent CdSe QDs contributed significantly to the enhanced photocatalytic H_2 evolution performance of the Au/CdSe superparticles.

Recently, Dong et al. prepared self-assembled superparticles of Fe_3O_4 NPs with doped TiO_2 nanorods by using the surfactant-assisted self-assembly (Xue et al., 2018). They found that the superparticles exhibit highly enhanced electrochemical properties, such as high specific capacity, rate capacity, and stable cycle performance of lithium storage. The significantly enhanced performance resulted from the synergistic effect between the co-assembled Fe_3O_4 NPs. First, the co-assembled Fe_3O_4 NPs improved the poor conductivity of TiO_2 superparticles. Second, the Fe_3O_4 NPs with a higher theoretical capacity contributed to the capacity of superparticles. Finally, the porosity and stability of the TiO_2 matrix provided enough stable void space to buffer the volume expansion of the Fe_3O_4 NPs, which improved cycling stability.

This surfactant-assisted emulsion method has been adopted to a variety of other complex NP systems, such as Au-gamma-Fe_2O_3 (Shang et al., 2017), PbS-gamma-Fe_2O_3 (Ortgies et al., 2016), magnetic Au NPs (Wang et al., 2018c), Au-CeO_2 (Chen et al., 2011), and zinc ferrite NPs (Park et al., 2017). Overall, the method shows versatility in the synthesis of new types of active superparticles from different NP building blocks.

Formation of Nanorod Superparticles

In the above discussion, spherical NPs have been very well demonstrated in the surfactant-assisted self-assembly process for synthesis of superparticles. By using multiple compositions of NPs, complex superparticles can also be readily produced to achieve multiple functions. It has been shown that nonspherical NPs, such as nanorods, can also be used for the synthesis of superparticles that exhibit anisotropic properties.

Cao et al. have reported the fabrication of ordered superparticles using highly luminescent CdSe-CdS core-shell nanorods as building blocks (Zhuang et al., 2009; Wang et al., 2012, 2013b; Banin and Sitt, 2012). The chloroform solution containing these hydrophobic nanorods is first mixed with an aqueous solution of DTAB followed by evaporation of chloroform to form water-soluble micelles. Then, the nanorod micelle solution was injected into ethylene glycol under vigorous stirring. This second step results in the loss of DTAB molecules into the growth solution, which leads to the aggregation of nanorods and the eventual formation of the 3D assembly structures. The resulting nanostructures have multiple well-defined supercrystalline domains with configurations

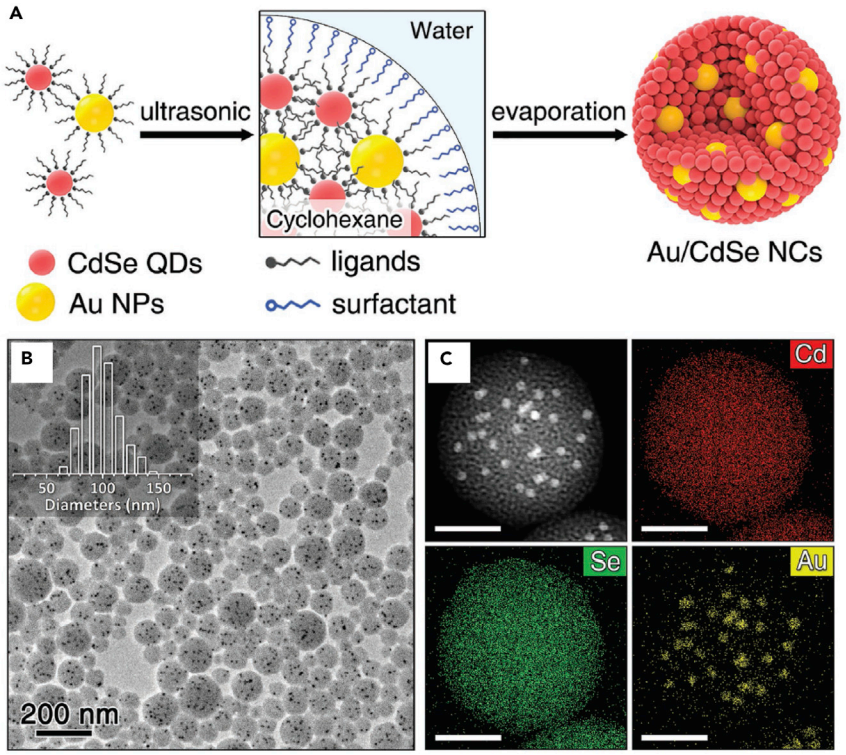

Figure 8. Multicomponent Superparticles Self-Assembled by Surfactant-Assisted Emulsion-Based Process

(A) Schematic illustration of the self-assembly process to synthesize the Au/CdSe superparticles.

(B and C) Transmission electron microscopic (B) and high-angle annular dark-field scanning transmission electron microscopy (HAADF-STEM) (C) images of Au/CdSe-0.15 superparticles (Au NPs size 7.2 nm) and corresponding energy dispersive spectroscopy (EDS) maps of Cd, Se, and Au. Inset in (B) shows the size distribution of as-prepared Au/CdSe superparticles. Scale bars, 50 nm in (C).

Reprinted with permission from Shi et al. (Shi et al., 2017). Copyright 2017 John Wiley & Sons, Inc.

and sizes that are dependent on the total number (N) of constituent nanorods in each nanostructure (Figure 9). The 3D double-domed cylindrical structure is obtained when N is less than ~80,000. This double-domed cylinder consists of seven distinct domains wherein the nanorods within a single domain are arranged parallel to each other, whereas the nanorods of neighboring domains are arranged normal to each other. Interestingly, it was found that when the nanorods are incubated with octylamine before micelle preparation, 3D needle-like nanostructures having only one supercrystalline domain are obtained. It has been demonstrated that when unidirectionally aligned in polydimethylsiloxane thin films, these 3D needles exhibit anisotropic PL property with strong linearly polarized emissions. This anisotropic optical property is believed to be caused by resonance energy transfer through dipole-dipole interactions within the self-assembled CdSe-CdS nanorods. These specific anisotropic nanostructures display great promise as downconversion phosphors for polarized light-emitting diodes. In addition to CdSe-CdS nanorods, $PbSeO_3$ nanorods have also been demonstrated for the formation of nanorod superparticles (Bai et al., 2007).

These results show that anisotropic interactions of nanorods can be used to synthesize superparticles with multiple well-defined supercrystalline domains. The anisotropic interactions between these nanorods can be kinetically introduced during self-assembly, leading to the formation of anisotropic assembled structures. It is anticipated that these findings can be extended for the self-assembly of nanomaterials having other anisotropic shapes, as well as the self-assembly of two or more types of anisotropic nanomaterials into well-defined mesoscopic and macroscopic complex architectures.

Microemulsion-Confined Self-Assembly of Porphyrins

Another flexible use of the surfactant-assisted self-assembly method is to assemble photoactive macromolecules, such as porphyrins, into nanocrystalline superparticles. Porphyrins and their derivatives have

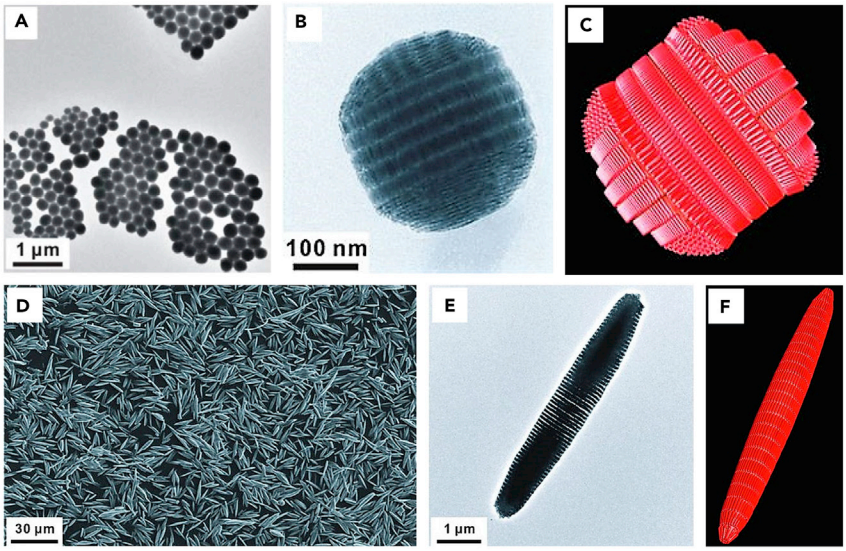

Figure 9. Formation of Nanorod Superparticles

(A–C) (A) Transmission electron microscopic (TEM) overview of 3D double-domed cylindrical superparticles made from CdSe/CdS semiconductor nanorods, (B) TEM zoom, and (C) model of the double-domed superparticle microstructure. (D) Scanning electron microscopic overview of needle-like superparticles formed by CdSe/CdS semiconductor nanorods. (E and F) (E) TEM zoom and (F) model of the needle-like superparticle microstructure.

Reproduced with permission from Wang et al. (Wang et al., 2012). Copyright 2012 AAAS.

macrocyclic π-conjugated ring structures, which exist as a 2D plane with side length of several nanometers (Zang et al., 2008). The well-defined conjugated electron structure gives them unique optical and electrical properties at the visible spectrum (Zhao et al., 2010; Ladomenou et al., 2015; Chen et al., 2016; Duong Duc et al., 2017; Zhang et al., 2017b; Yella et al., 2011; Mathew et al., 2014). Also, their rigid and planar molecular skeleton and inherent aromatic electronic features facilitate their self-assembly into well-defined nanostructures with favorable optoelectronic properties (Zhong et al., 2014b). Self-assembly of these conjugated molecules results in densely packed nanocrystalline superparticles or networks that enable highly efficient charge and energy transfer for enhanced optoelectronic properties and collective behaviors (Hasobe, 2013).

In recent years, various porphyrin nanocrystalline superparticles with uniform shape and size have been produced by using the surfactant-assisted self-assembly method, including hollow nanospheres, solid nanospheres, nanotubes, nanorods, nano-octahedra, nanosheets, and nanofibers (Zhong et al., 2014b; Qiu et al., 2010; Guo et al., 2012a, 2012b, 2013; Fruehbeisser and Groehn, 2012; Chen et al., 2014). Bai et al. demonstrated the formation of superparticles with well-defined morphology by using hydrophobic tin (IV) meso-tetraphenylporphine dichloride porphyrin (Figure 10) (Zhong et al., 2014b). In their preparation, chloroform solution containing tin porphyrin was added to an aqueous solution of CTAB or SDS surfactants. This solution was then emulsified by ultrasonic treatment under gentle stirring. The low-boiling chloroform was subsequently evaporated from the emulsion system by mild heating. As chloroform evaporates from the emulsion droplets, they are enriched in concentration, and this induces self-assembly of porphyrin molecules confined in the emulsion droplets. Through noncovalent interactions, such as π-π stacking and ligand coordination, tin porphyrins self-assembled into different nanostructures.

The growth process of the nanocrystals is an evaporation-induced nucleation and growth self-assembly mechanism. At the beginning of the self-assembly processes when oil and water phases are mixed together, emulsion droplets are rapidly formed. As the self-assembly progresses during heating, the emulsion droplets gradually shrink. This shrinkage is due to the evaporation of the organic solvent with heating. The evaporation in the first few minutes resulted in small NP nuclei. Then the nuclei started to grow quickly into nanocrystalline superparticles with controllable size and shape.

Bai et al. discovered that the type of surfactant was a key factor to the control of morphologies and arrangement of the porphyrins. For example, when CTAB was used, nanocrystalline octahedra were obtained.

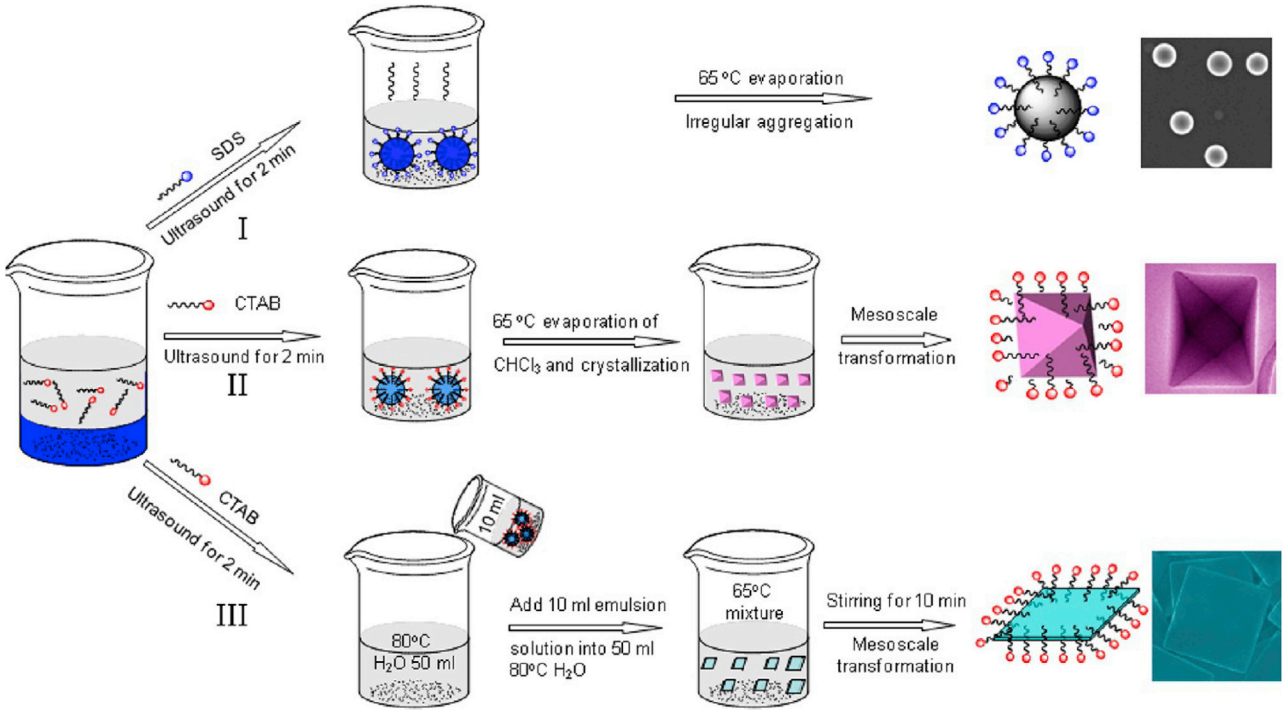

Figure 10. Schematic Illustration of the Synthesis Processes of Porphyrin Nanocrystals by the Surfactant-Assisted Cooperative Self-Assembly Method

Reprinted with permission from Zhong et al. (Zhong et al., 2014b). Copyright 2014 American Chemical Society.

When CTAB was replaced with SDS under the same self-assembly conditions, amorphous microspheres were formed instead of octahedra. It is believed that the different nanocrystalline morphologies are due to the nature of interactions of surfactants with porphyrins. In the case of SDS, the anionic head groups SO_4^{2-} of SDS might bind with the central Sn at the core of the porphyrin molecules, which prohibits tin porphyrin self-assembly through noncovalent interactions. The evaporation of organic solvents resulted in amorphous microspheres instead of crystalline octahedra. Besides the morphology, the size of the tin porphyrin self-assembled nanocrystals can be easily tuned by varying the surfactant concentration. By increasing the CTAB concentration, diameters of porphyrin octahedral nanocrystals increased from 85 to 440 nm, whereas their polydisperse index remained narrow.

Similar to the formation of spherical NP superparticles during surfactant-assisted self-assembly, temperature also has a big impact on the self-assembly and formation of porphyrin nanocrystals. For example, at the same self-assembly conditions, evaporation at 80°C resulted in nanosheets with edge length ranging from 300 to 500 nm. The relative amount of the octahedra to the nanosheets decreased with an increase of temperature. This might be due to the preferential formation of CTAB lamellar mesophase, which confines formation of the nanosheet morphology.

The additional morphologies and structure control of the porphyrin nanocrystals benefit mainly from the intermolecular forces between the porphyrin and surfactants compared with the spherical NP self-assembly discussed above. Besides van der Waals forces, additional noncovalent interactions between surfactant and porphyrin, such as hydrogen bonding, aromatic π-π stacking, and axial coordination, provide rich options for forming different morphologies and sizes during the self-assembly process. For example, in the tin porphyrin octahedral nanocrystals, the porphyrin macrocycles lie flat in the a-b plane with the core Sn at the corners and centers of the unit cells. As such, each porphyrin has 12 neighbors with which it interacts, 8 neighbors offset above and below its plane (stronger interactions) and 4 neighbors in-plane (weaker interactions). Periodic semiempirical calculations (PM6) find the crystal binding energy to be 72 kJ/mol, which is far greater than the energy of thermal motion. This indicates that the self-assembly process is controlled by molecular interaction other than thermodynamics that occur in the NP systems, which results in diverse morphologies compared with NP assembly systems.

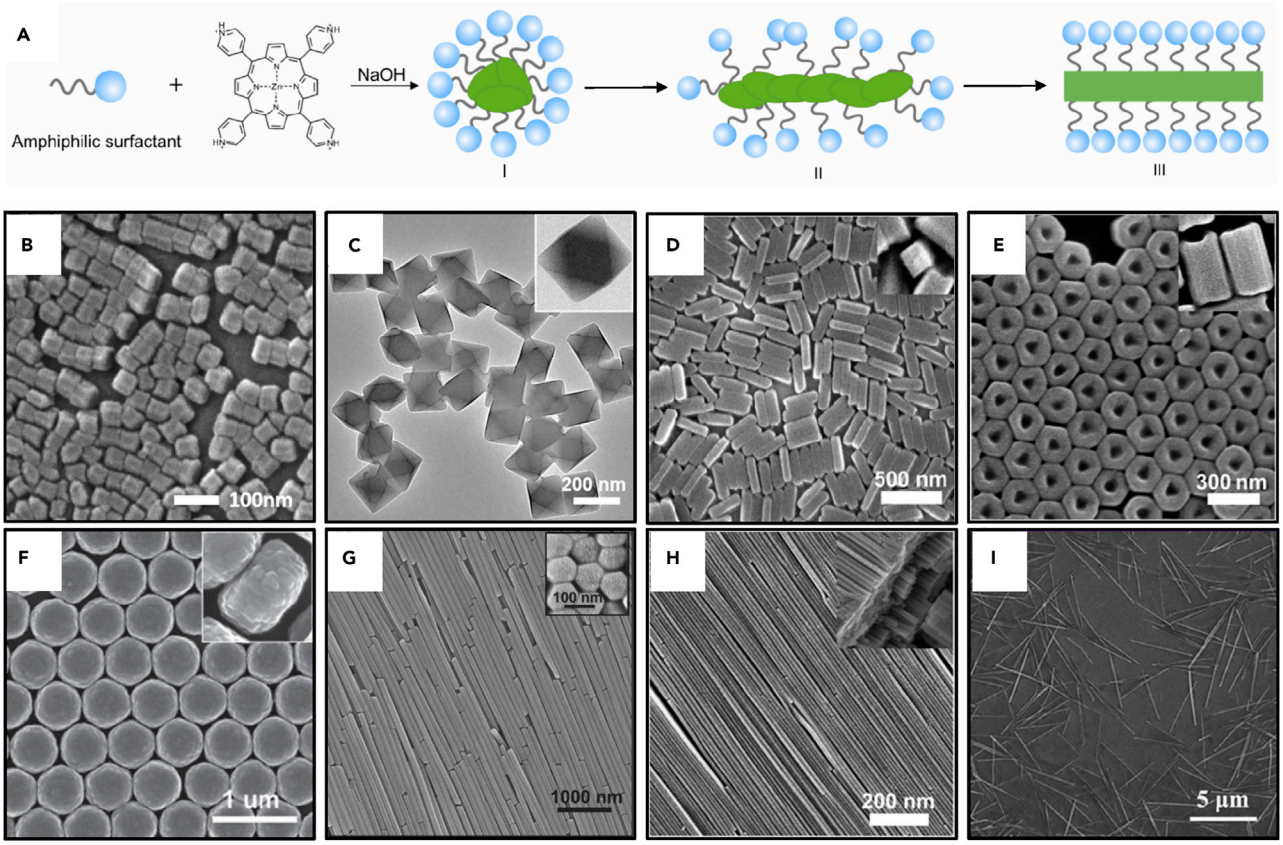

Figure 11. Scanning and Transmission Electron Microscopic Images of the Porphyrin Nanocrystals with Different Shapes and Sizes

(A–I) (A) Schematic illustration of formation of the self-assembled porphyrin nanostructures. (B) NPs, (C) nano-octahedra, (D) tetragonal nanorods, (E) hexagonal nanorods, (F) nanodisks, (G) hexagonal nanowires, (H) short nanowires, and (I) long nanowires. (A and D) Reproduced with permission from Zhong et al. (Zhong et al., 2014a). Copyright 2014 American Chemical Society. (B) Reproduced with permission from Wang et al. (Wang et al., 2018b). Copyright 2018 American Chemical Society. (C and G) Reproduced with permission from Wang et al. (Wang et al., 2016). Copyright 2016 American Chemical Society. (E and H) Reproduced with permission from Bai et al. (Bai et al., 2011). Copyright 2011 American Chemical Society. (F) Reproduced with permission from Bai et al. (Bai et al., 2010). Copyright 2010 of the Royal Society of Chemistry. (I) Reproduced with permission from Zhang et al. (Zhang et al., 2018). Copyright 2018 American Chemical Society.

Inspired by the original concept of the surfactant-assisted self-assembly approach, a modified process was developed to fabricate self-assembled porphyrin nanocrystals (Bai et al., 2010, 2011). Some porphyrins, such as zinc meso-tetra (4-pyridyl) porphyrin (ZnTPyP), are hard to dissolve in common organic solvents such as chloroform and toluene. Therefore it is impossible to apply the surfactant-assisted self-assembly directly. Bai et al. modified the method through an acid-base neutralization process in the aqueous phase instead of forming microemulsions. In this case, they were able to self-assemble ZnTPyP into more favorable arrangements via coordination of its peripheral pyridine groups to its core Zn ions, whereas most porphyrins form H-aggregates in a face-to-face manner via π-overlap (Zhong et al., 2014a). First, they protonated ZnTPyP with positive charges through an acidic solution to prepare a water-soluble precursor. Then, they mixed the acidic aqueous solution with a basic surfactant solution under vigorous stirring with a range of volume ratios. Once mixed, acid-base neutralization reaction occurred and deprotonated the charged ZnTPyP precursor. This produced insoluble neutral ZnTPyP molecules that were automatically trapped into the hydrophobic micellar interiors. Through confined noncovalent interactions within surfactant micelles, such as metal-ligand axial coordination (Zn-N) and π-π interactions, nucleation and growth was initiated for the formation of nanocrystals with a series of morphologies with controlled sizes and dimensions. The role of the surfactants is to essentially encapsulate hydrophobic porphyrins within the surfactant micellar interiors, which further confines the self-assembly of the ZnTPyP nanocrystals. Using this modified method, various 1D–3D porphyrin nanocrystals such as NPs, nanooctahedra, hexagonal rods, tetragonal nanorods, nanotubes, nanowires, and nanodisks have been produced through kinetic control (Figure 11)

(Zhong et al., 2014a; Wang et al., 2016, 2017, 2018b; Zhang et al., 2018). For example, the nanocrystal dimension increases with increasing surfactant concentrations and pH value.

Besides ZnTPyP porphyrin, the modified method has been successfully extended to assemble other porphyrins into nanocrystalline superparticles, such as meso-tetra(4-pyridyl) porphine (H_2TPyP) or 5,10,15,20-tetrakis(4-(hydroxyl)phenyl) porphyrin (THPP) (Wang et al., 2016; Zhang et al., 2018). The assembly of H_2TPyP is initiated by adding the protonated porphyrin tetraammonium salt acidic aqueous solution into the basic solution of surfactant under vigorous stirring. The mixture of protonated porphyrins and the base solution immediately triggers an acid-base neutralization reaction that deprotonates pyridine tetraammonium salt, producing neutral porphyrins that are insoluble in water. The resulting insoluble porphyrins are then encapsulated into the hydrophobic cores of surfactant micelles. This encapsulation then confines the nucleation and growth driven by noncovalent interactions such as π-π stacking, forming uniform porphyrin NPs. Notably, metalation of the porphyrin can be realized during the assembly process by the addition of Zn^{2+} (through $Zn(NO_3)_2$) in the self-assembly solution (Wang et al., 2016). Zn is inserted into the core of H_2TPyP through the incorporation of Zn ions with the core pyrroles forming ZnTPyP. Subsequent self-assembly of ZnTPyP was conducted through axial ligation between central Zn and pyridyl groups, which results in the morphology changing from octahedron to nanowires.

In the case of THPP self-assembly, THPP was first alkalized to make a water-soluble precursor (Zhang et al., 2018). Although THPP has four hydroxyl groups at the outer core of the porphyrin, it is not soluble in water. To initiate the self-assembly in aqueous phase, it is first alkalized so that its hydroxyl groups are deprotonated to form tetrahydroxy TPP^{4-} anions that are soluble in water solutions. Then the TPP^{4-} basic solution was added into an acidic surfactant solution under vigorous stirring to initiate the acid-base neutralization reaction. The four hydroxyl groups were recovered from the corresponding anion state, whereas the two nitrogen groups at the inner core of the THPP were protonated, forming $(H_2THPP)^{2+}$, which is encapsulated within the hydrophobic interior of the surfactant micelles. Consequently, the combined noncovalent interactions such as hydrophobic-hydrophobic, hydrogen bonding, and aromatic π-π stacking induce nucleation and growth, and the eventual formation of self-assembled 1D THPP nanostructures within the micelles.

APPLICATIONS

The surfactant-assisted cooperative self-assembly method achieves well-defined active nanomaterial structures and properties by confining the NP self-assembly or growth within nanocompartments such as micelles and emulsions. The interdigitated surfactant or phospholipid bilayer nanostructure provides a water-soluble and biocompatible interface for biomedical applications such as imaging (Fan et al., 2005b; Dubertret et al., 2002) and drug delivery (Kim et al., 2006). Owing to the confined self-assembly, highly ordered and densely packed NP nanostructures have been produced. The ordered structure results in new collective properties and enhanced charge and energy transport for applications in photocatalysis and nanoelectronic devices. For example, self-assembly enables effective optical coupling of porphyrins, resulting in more enhanced optical absorption when compared with the original porphyrin monomers. The absorption bands also red shift to a more extensive visible light spectrum. The self-assembled porphyrin network facilitates efficient energy transfer among porphyrin molecules and the delocalization of excited state electrons for enhanced photocatalytic hydrogen production under visible light (Zhang et al., 2018; Wang et al., 2016; Zhong et al., 2014a, 2014b). By using multi-compositional NPs as the building block, highly ordered superparticles possess multiple functions that depend on the choice of the initial NPs for a number of interesting applications such as biomedical, photocatalytic, and optic/electric devices (Lu and Yin, 2012). For example, self-assembling magnetic iron oxide into superparticles increases the saturation magnetization, while avoiding the superparamagnetic-ferromagnetic transition (Ge et al., 2007). The monodisperse, highly water-soluble, superparamagnetic, and biocompatible magnetite nanocrystals should find immediate important biomedical applications.

Biomedical Applications

The interdigitated bilayers provide an effective interface and enable NPs to be water soluble and biocompatible for biological applications such as imaging and photodynamic therapy (PDT)/photothermal therapy. Chen et al. reported the synthesis of colloidal magnetofluorescent superparticles by co-assembling magnetic NPs with fluorescent QDs (Chen et al., 2014). The final superparticles consist of a close-packed magnetic NP "core" that is fully surrounded by a "shell" of fluorescent QDs (Figure 12). The superstructure

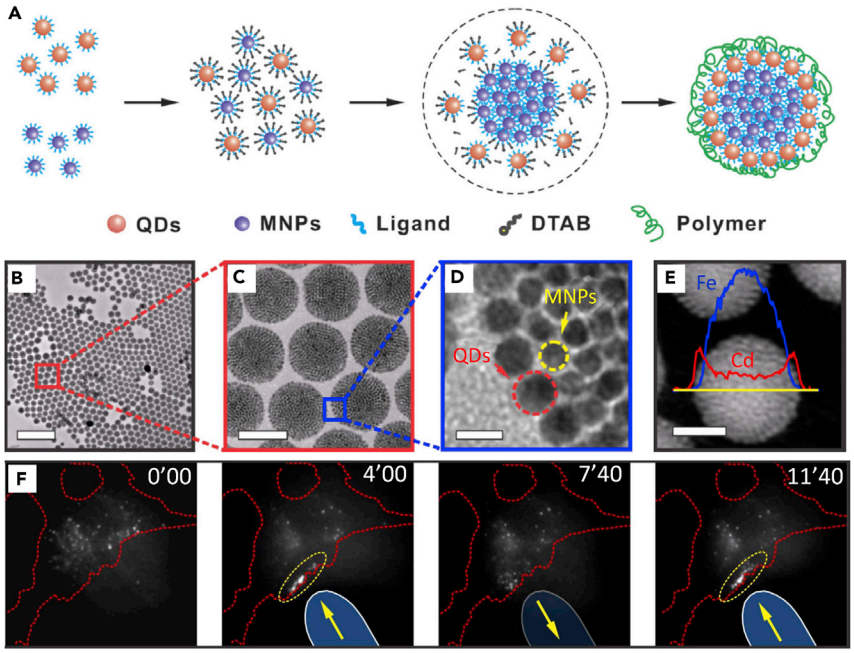

Figure 12. Formation of Magnetic-Fluorescent Superparticles for Biological Applications

(A) Schematic of the formation of the magnetic-fluorescent superparticles.

(B–D) Transmission electron microscopic images of magnetic-fluorescent superparticles at different magnifications. Scale bars, 500 nm in (B), 100 nm in (C), and 10 nm in (D).

(E) EDS elemental line scan result. Scale bar, 60 nm.

(F) Intravital multiphoton microscopic picture of a HeLa cell in which magnetic-fluorescent superparticles have been microinjected. By bringing the magnetic tip in and out (blue bars), a reversible accumulation of magnetic-fluorescent superparticles (yellow region) can be created at the cell periphery (indicated by red dashed line) at different time points. Reproduced by permission from Chen et al. (Chen et al., 2014). Copyright 2014 Macmillan Publishers Ltd.

exhibits uniform and tunable sizes, high magnetic content loading, and maximized fluorophore loading on the surface and versatile surface functionality. The superparticles can be further encapsulated with a thin silica shell through a sol-gel process to improve biocompatibility and colloidal stability. No measureable changes in both the PL intensity and size were observed after 6 months at 4°C. They demonstrated that after surface pegylation, these magnetofluorescent superparticles could be magnetically manipulated inside living cells while being optically tracked. Moreover, these magnetofluorescent superparticles also served as an *in vivo* multiphoton and MR dual-modal imaging probe.

Wang et al. synthesized self-assembled porphyrin-silica nanocomposite particles with an ordered porphyrin network as the core surrounded by amorphous silica as the shell for a high-yield generation of singlet oxygen for PDT (Wang et al., 2017). The long-range ordering of the porphyrin network enables efficient energy transfer and impressive fluorescence for cell labeling while the silica layer provides opportunities for biofunctionalization. The synthesis of these particles was conducted by the combined surfactant-assisted cooperative self-assembly and sol-gel process using silicate precursors and the photoactive precursor zinc porphyrin ZnTPyP as a building block (Figure 13). Control of pH conditions in the self-assembly solution is an important factor for tuning the final nanostructures with either amorphous or crystalline porphyrin networks. Low pH conditions promoted porphyrin noncovalent self-assembly, forming core-shell particles. However, high pH conditions were favorable for silicate condensation, forming solid porphyrin-silica mesophase particles. Both types of nanocomposites can generate lethal singlet oxygen to kill HeLa cells, but the core-shell structured particles were found to have better singlet oxygen yield, which is probably due to the increased porphyrin π-π stacking and out-of-plane coordination of Zn and pyridine. The enhanced PDT activity was demonstrated in the phototherapy with more tumor cells destroyed by the core-shell structured particles, which is consistent with their high yield production of singlet oxygen.

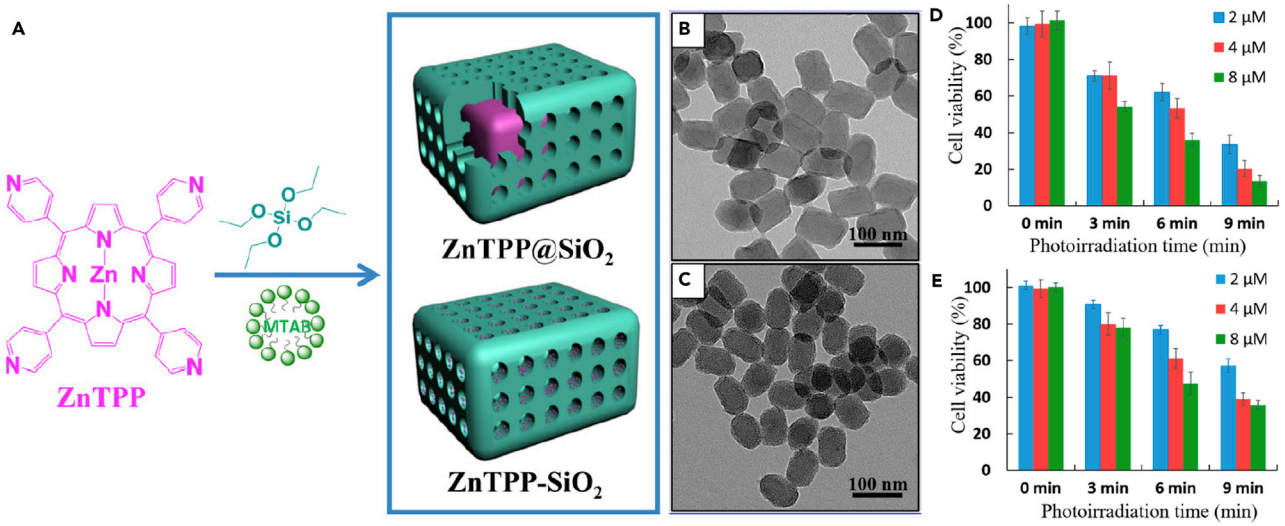

Figure 13. Formation of Core-Shell Structured ZnTPyP@SiO2 and Solid Mesophase ZnTPyP-SiO2 Nanocomposite Particles for PDT

(A) Schematic diagram for the controlled formation of core-shell structured ZnTPyP@SiO2 and solid mesophase ZnTPyP-SiO2 nanocomposite particles.

(B and C) Transmission electron microscopic images of the corresponding nanocomposite particles, respectively.

(D and E) Relative viability of HeLa cells after treating with the corresponding nanocomposite particles, respectively.

Reproduced with permission from Wang et al. (Wang et al., 2017). Copyright 2017 American Chemical Society.

One important feature in this assembly process is the formation of an interdigitated bilayer structure of surfactants and lipids on the surface of the assemblies, which adds active interface for water-solubility and for biomedical applications, as discussed above.

Photocatalysis

One important issue in the synthesis of photocatalytic materials is to increase photoactive material absorption in the visible light range and hot-electron transport to the reaction sites. One method to address these issues is to assemble optically active nanomaterials into highly ordered structures to increase their absorption cross-section and hot-electron transport. Zhong et al. found that the absorption spectra of self-assembled porphyrin nanocrystals are more broad in the visible wavelength when compared with those of individual porphyrins and display enhanced photocatalytic activity compared with commercial P25 catalysts (Chen et al., 2014). They also found that the extent of self-assembly caused different morphology-dependent photocatalytic activity. Similarly, H_2TPyP nanowires and H_2TPyP octahedra exhibit much broader UV-vis absorption bands that are red shifted and enhanced from the corresponding bands of the monomeric porphyrins (Wang et al., 2016). Under visible light ($\lambda > 420$ nm) irradiation with ascorbic acid as the sacrificial agent and Pt as the co-catalyst, ZnTPyP nanowires displayed the highest hydrogen evolution rate of 47.1 mmol/g/h, which is much higher than the reported porphyrin- and other organic-material-based photocatalysts, whereas the H_2TPyP nanooctahedra exhibited negligible photocatalytic activity with an evolution rate of 0.8 mmol/g/h. This extraordinary photocatalytic activity mainly benefits from the long axes of π-π stacks in the 1D nanostructures that have extensive delocalization and retard the charge recombination by stabilizing the electron transfer products, which enhances the lifetime of electron-hole pairs.

A detailed research was reported on self-assembled THPP nanorods and nanowires for photocatalytic generation of hydrogen by Zhang et al. (Figure 14) (Zhang et al., 2018). Based on results of X-ray diffraction (XRD) patterns and UV-vis absorption spectra, they found that the formation of J-aggregate leads to much stronger exciton coupling between THPPs. Such coupling activates the porphyrin core by increasing the electronic density to a large extent, which helps to stabilize the photoexcited electron-holes for enhanced hydrogen evolution rate of all nanowires. Such arrangement is similar to that of a light-harvesting complex in natural photosynthetic systems that contain chlorophyll aggregates, in which chromophores form J-aggregates along the head-to-tail arrangement via a stronger transition-dipole moment for

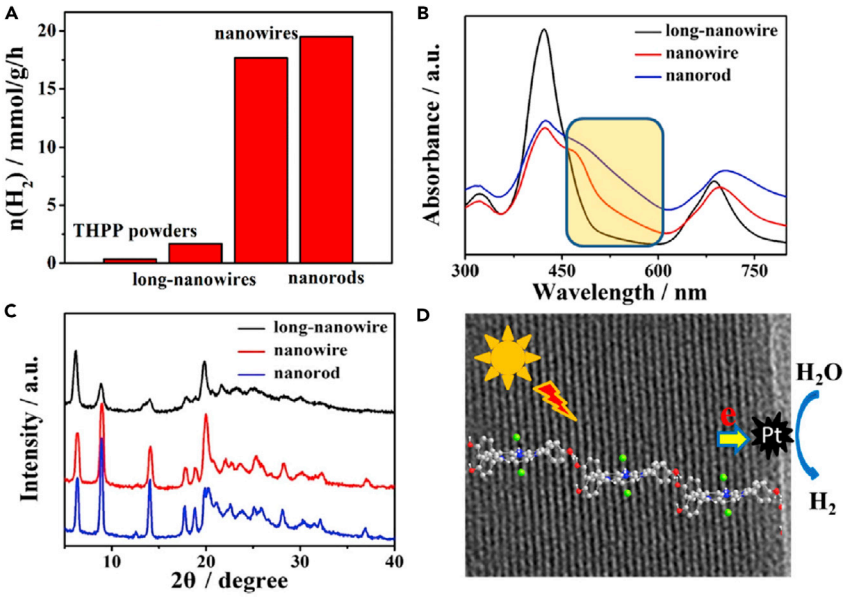

Figure 14. Photocatalytic Hydrogen Production and Characterizations of the THPP Powders and Different Self-Assembled THPP Nanostructures

(A) Hydrogen evolution photocatalyzed by THPP powders and different self-assembled nanostructures.

(B) UV-vis spectra of different self-assembled THPP nanostructures.

(C) XRD of different nanostructures.

(D) Schematic illustration of the self-assembled J-aggregates and photo-induced charge process for hydrogen generation.

Reprinted with permission from Zhang et al. (Zhang et al., 2018). Copyright 2018 American Chemical Society.

harvesting solar energy. In addition, the absorption spectroscopy results unambiguously establish that a self-assembled nanostructure induces different coverage of the light range of spectra, which results in structure-dependent photocatalytic hydrogen evolution activity (Figures 14A and 14B). Shorter nanorods or nanowires exhibited much better photocatalytic performance than long nanowires (Figure 14A). From XRD patterns (Figure 14C), they found that the nanorods have decreased separation distance of the porphyrin lattice fringes (Figure 14D). This essentially increases the interactions between THPP molecules within nanorods, which enhances the delocalization of excited electrons and extends the lifetime of electron-hole pairs for better photoactivity.

Nanoelectronic Devices

The surfactant-assisted cooperative self-assembly enables formation of highly ordered and densely packed NP arrays for collective behavior and enhanced charge transport. In general, such highly ordered NP arrays should serve as ideal model systems to discover new nanoscale phenomena, and to develop and test theories of collective optical, electronic, and magnetic behaviors. Fan et al. reported the synthesis of planar metal-insulator-metal devices from ordered 3D mesophases consisting of gold NPs inside silica matrix (Fan et al., 2004; Yang et al., 2005). Charge transport studies within the thin-film gold NP/silica arrays showed that at room temperature, the *I-V* behavior was linear. Nonlinearity near zero bias was evident at 200 K and increased with decreasing temperature. At 100 K and below, conduction occurred through the gold NC/silica insulator only above a minimum threshold voltage V_T, indicative of a collective Coulomb blockade resulting from electrical isolation of the NPs. For such arrays of Coulomb islands, theory predicts that for $V>V_T$, current scales as the power law, $I=I_0(V/V_T-1)^{\zeta}$, and that the value of the scaling exponent ζ reflects the dimensionality of the accessible current-conducting pathways. Linear Arrhenius behavior of the zero bias conductance from 78 K to room temperature testified to the uniformity of NP sizes and interparticle spacings. The calculated activation energy U = 90.4meV is attributed to the Coulomb charging energy of individual gold NPs. By measuring the *I-V* characteristics at T greater than the threshold temperature, the current voltage scaling relationship for a well-defined 3D NP array $I \sim V^{2.9}$ was established for the first time (Figure 15).

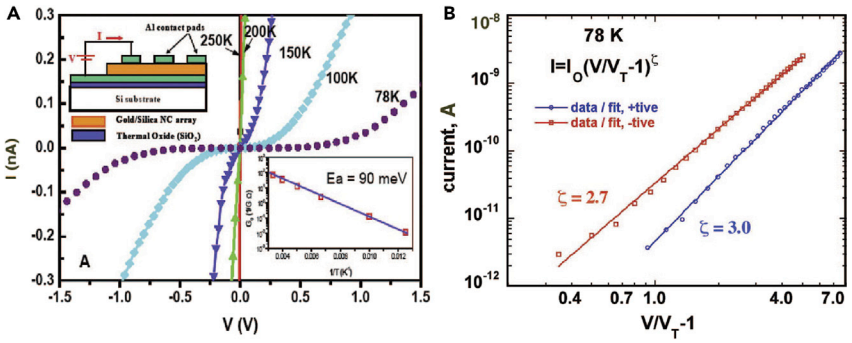

Figure 15. Charge Transport in Thin Film of Gold NP/Silica Arrays

(A) I-V curves measured from 300 to 78 K. The inset shows a plot of the zero-bias conductance (*G0*) versus *1/T*. The data exhibited Arrhenius behavior with activation energy (*Ea*) of ~90 meV.

(B) At T = 78 K, the current displayed a power-law dependence for V > VT with scaling exponent ζ = 2.7 (negative bias) and ζ = 3.0 (positive bias).

Reproduced with permission from Fan et al. (Fan et al., 2004). Copyright 2004 AAAS.

Conclusion and Outlook

In summary, recent research progress on the surfactant-assisted cooperative self-assembly of NPs to form highly ordered active nanostructures has been reviewed. A variety of nanomaterials including plasmonic NPs, fluorescent semiconductors, magnetic NPs, and optical active molecules have been assembled into highly ordered active NP nanostructures. Benefiting from the flexible composition, ordered structure, and biocompatible properties, these nanostructures have been utilized in the areas of nanoelectronics, photocatalysis, and biomedicine. One of the advantages of the surfactant-assisted self-assembly method is its ability to integrate different functional nanomaterials to create active superparticles with multiple functions. Another important advantage is that the resultant nanostructures exhibit new collective properties resulting from the self-assembled and compactly packed NPs, which enhances charge and energy transport within the nanostructures.

Although great success has been achieved in the development of surfactant-assisted assembly strategies for the synthesis of highly ordered NP active nanostructures, accurate control of structure and property of the final nanostructures still remains a great challenge. This requires precise control of size, shape, and composition of the starting building block of different nanomaterials. Establishment of structure-property relation for the final nanostructures through surfactant-assisted self-assembly will further improve the understanding of the surfactant-assisted self-assembly processing for better design and engineering of active nanostructures. There has been an emergence of new nanomaterials, such as graphene and its derivatives (Taheri Najafabadi, 2015), perovskite nanomaterials (Hills-Kimball et al., 2017), and transition-metal dichalcogenides (Manzeli et al., 2017), such as MoS_2, and $MoSe_2$, that have been extensively explored for important applications in nanoelectronics and optoelectronics, energy conversion and storage, photocatalysis, and biomedicines (Lai et al., 2016). These nanomaterials will benefit from the surfactant-assisted self-assembly to form highly ordered and compacted nanostructures with enhanced properties. For example, compact QD thin films are one of most important prerequisites for high-performance perovskite QD solar cells, which ensures efficient electronic coupling between QDs for effective carrier transport (Tang et al., 2011; Swarnkar et al., 2016; He et al., 2017a; Meidan et al., 2017). Although using short inorganic ligands can obviously reduce the interparticle spacing to enhance electronic coupling, it is still challenging to transfer randomly stacked QD films into regular arrays for better carrier transport (Sanehira et al., 2017; He et al., 2017a; Meidan et al., 2017). Therefore high-quality QDs' growth and self-assembly of QD thin film are the most fundamental steps for the efficient perovskite QD solar cells. To this end, surfactant-assisted self-assembly strategy can achieve more compact film configuration for stronger electronic coupling and charge mobility by building high-quality self-assembled QD films and reducing interparticle spacing among QDs. Recently, direct assembly such as stress-induced assembly has been developed to tune NP phase transformation and coupling (Jiang et al., 2016; Quan et al., 2011, 2013; Wang et al., 2015; Nagaoka et al., 2017; Zhu et al., 2017). It also requires ordered NP assemblies as the starting materials to accomplish the stress-induced tuning of phase transition and interparticle separation. Another interesting direction in the NP community is the synthesis of hybrid nanocrystals

through nanocrystal or ion diffusion in solutions to control nano-heterogeneous structures (Cozzoli et al., 2006; Ghosh and Manna, 2018; Zhang et al., 2017a; Pang et al., 2013, 2016; Erwin et al., 2005). Finally, increasing structural complexity by combining with other top-down and bottom-up methods is one of the natural directions for nanoscience. It is expected that new complex active nanostructures will be synthesized through surfactant-assisted self-assembly for exploration of novel applications (Dai et al., 2016; Sun et al., 2017; Liao et al., 2014; Pang et al., 2013, 2016).

ACKNOWLEDGMENT

H.F. acknowledges partial support from the Center for Integrated Nanotechnologies (CINT), an Office of Science User Facility operated for the US Department of Energy Office of Science. F.B. acknowledges support from the National Natural Science Foundation of China (21771055, U1604139, 21422102, 21403054), Plan for Scientific Innovation Talent of Henan Province (No. 174200510019), and Program for Changjiang Scholars and Innovative Research Team in University (No. PCS IRT_15R18). Sandia National Laboratories is a multimission laboratory managed and operated by National Technology and Engineering Solutions of Sandia, LLC., a wholly owned subsidiary of Honeywell International, Inc., for the US Department of Energy's National Nuclear Security Administration under contract DE-NA0003525.

REFERENCES

Bai, F., Sun, Z., Wu, H., Haddad, R.E., Coker, E.N., Huang, J.Y., Rodriguez, M.A., and Fan, H. (2011). Porous one-dimensional nanostructures through confined cooperative self-assembly. Nano Lett. *11*, 5196–5200.

Bai, F., Wang, D., Huo, Z., Chen, W., Liu, L., Liang, X., Chen, C., Wang, X., Peng, Q., and Li, Y. (2007). A versatile bottom-up assembly approach to colloidal spheres from nanocrystals. Angew. Chem. Int. Ed. *46*, 6650–6653.

Bai, F., Wu, H., Haddad, R.E., Sun, Z., Schmitt, S.K., Skocypec, V.R., and Fan, H. (2010). Monodisperse porous nanodiscs with fluorescent and crystalline wall structure. Chem. Commun. (Camb). *46*, 4941–4943.

Banin, U., and Sitt, A. (2012). Colloidal self-assembly superparticles get complex. Nat. Mater. *11*, 1009–1011.

Bian, K., Schunk, H., Ye, D., Hwang, A., Luk, T.S., Li, R., Wang, Z., and Fan, H. (2018). Formation of self-assembled gold nanoparticle supercrystals with facet-dependent surface plasmonic coupling. Nat. Commun. *9*, 2365.

Bigall, N.C., Parak, W.J., and Dorfs, D. (2012). Fluorescent, magnetic and plasmonic-Hybrid multifunctional colloidal nano objects. Nano Today *7*, 282–296.

Boles, M.A., Engel, M., and Talapin, D.V. (2016). Self-assembly of colloidal nanocrystals: from intricate structures to functional materials. Chem. Rev. *116*, 11220–11289.

Chen, C., Nan, C., Wang, D., Su, Q., Duan, H., Liu, X., Zhang, L., Chu, D., Song, W., Peng, Q., and Li, Y. (2011). Mesoporous multicomponent nanocomposite colloidal spheres: ideal high-temperature stable model catalysts. Angew. Chem. Int. Ed. *50*, 3725–3729.

Chen, O., Riedemann, L., Etoc, F., Herrmann, H., Coppey, M., Barch, M., Farrar, C.T., Zhao, J., Bruns, O.T., Wei, H., and Guo, P. (2014). Magneto-fluorescent core-shell supernanoparticles. Nat. Commun. *5*, 5093.

Chen, Y., Li, A., Huang, Z.-H., Wang, L.-N., and Kang, F. (2016). Porphyrin-based nanostructures for photocatalytic applications. Nanomaterials *6*, 51.

Cozzoli, P.D., Pellegrino, T., and Manna, L. (2006). Synthesis, properties and perspectives of hybrid nanocrystal structures. Chem. Soc. Rev. *35*, 1195–1208.

Dai, X., Wu, J., Qian, Z., Wang, H., Jian, J., Cao, Y., Rummeli, M.H., Yi, Q., Liu, H., and Zou, G. (2016). Ultra-smooth glassy graphene thin films for flexible transparent circuits. Sci. Adv. *2*, e1601574.

de Nijs, B., Dussi, S., Smallenburg, F., Meeldijk, J.D., Groenendijk, D.J., Filion, L., Imhof, A., van Blaaderen, A., and Dijkstra, M. (2015). Entropy-driven formation of large icosahedral colloidal clusters by spherical confinement. Nat. Mater. *14*, 56–60.

Dubertret, B., Skourides, P., Norris, D.J., Noireaux, V., Brivanlou, A.H., and Libchaber, A. (2002). In vivo imaging of quantum dots encapsulated in phospholipid micelles. Science *298*, 1759–1762.

Duong Duc, L., Bhosale, S.V., Jones, L.A., and Bhosale, S.V. (2017). Arginine-induced porphyrin-based self-assembled nanostructures for photocatalytic applications under simulated sunlight irradiation. Photochem.Photobiol. Sci. *16*, 151–154.

Erwin, S.C., Zu, L., Haftel, M.I., Efros, A.L., Kennedy, T.A., and Norris, D.J. (2005). Doping semiconductor nanocrystals. Nature *436*, 91–94.

Fan, H. (2008). Nanocrystal-micelle: synthesis, self-assembly and application. Chem. Commun. (Camb). 1383–1394.

Fan, H., Wright, A., Gabaldon, J., Rodriguez, A., Brinker, C.J., and Jiang, Y.-B. (2006). Three-dimensionally ordered gold nanocrystal/silica superlattice thin films synthesized via sol-gel self-assembly. Adv. Funct. Mater. *16*, 891–895.

Fan, H.Y., Leve, E., Gabaldon, J., Wright, A., Haddad, R.E., and Brinker, C.J. (2005a). Ordered two- and three-dimensional arrays self-assembled from water-soluble nanocrystal-micelles. Adv. Mater. *17*, 2587–2590.

Fan, H.Y., Leve, E.W., Scullin, C., Gabaldon, J., Tallant, D., Bunge, S., Boyle, T., Wilson, M.C., and Brinker, C.J. (2005b). Surfactant-assisted synthesis of water-soluble and biocompatible semiconductor quantum dot micelles. Nano Lett. *5*, 645–648.

Fan, H.Y., Yang, K., Boye, D.M., Sigmon, T., Malloy, K.J., Xu, H.F., Lopez, G.P., and Brinker, C.J. (2004). Self-assembly of ordered, robust, three-dimensional gold nanocrystal/silica arrays. Science *304*, 567–571.

Fruehbeisser, S., and Groehn, F. (2012). Catalytic activity of macroion-porphyrin nanoassemblies. J. Am. Chem. Soc. *134*, 14267–14270.

Ge, J., Hu, Y., Biasini, M., Beyermann, W.P., and Yin, Y. (2007). Superparamagnetic magnetite colloidal nanocrystal clusters. Angew. Chem. Int. Ed. *46*, 4342–4345.

Ghosh, S., and Manna, L. (2018). The many "facets" of halide ions in the chemistry of colloidal inorganic nanocrystals. Chem. Rev. *118*, 7804–7864.

Gilroy, K.D., Ruditskiy, A., Peng, H.-C., Qin, D., and Xia, Y. (2016). Bimetallic nanocrystals: syntheses, properties, and applications. Chem. Rev. *116*, 10414–10472.

Gong, J., Newman, R.S., Engel, M., Zhao, M., Bian, F., Glotzer, S.C., and Tang, Z. (2017). Shape-dependent ordering of gold nanocrystals into large-scale superlattices. Nat. Commun. *8*, 14038.

Grzelczak, M., Vermant, J., Furst, E.M., and Liz-Marzan, L.M. (2010). Directed self-assembly of nanoparticles. ACS Nano *4*, 3591–3605.

Guo, P., Chen, P., and Liu, M. (2012a). Porphyrin assemblies via a surfactant-assisted method: from nanospheres to nanofibers with tunable length. Langmuir *28*, 15482–15490.

Guo, P., Chen, P., and Liu, M. (2013). One-dimensional porphyrin nanoassemblies assisted via graphene oxide: sheetlike functional surfactant and enhanced photocatalytic behaviors. ACS Appl. Mater. Interfaces *5*, 5336–5345.

Guo, P., Chen, P., Ma, W., and Liu, M. (2012b). Morphology-dependent supramolecular photocatalytic performance of porphyrin nanoassemblies: from molecule to artificial supramolecular nanoantenna. J. Mater. Chem. *22*, 20243–20249.

Hasobe, T. (2013). Porphyrin-based supramolecular nanoarchitectures for solar energy conversion. J. Phys. Chem. Lett. *4*, 1771–1780.

He, M., Li, B., Cui, X., Jiang, B., He, Y., Chen, Y., O'Neil, D., Szymanski, P., Ei-Sayed, M.A., Huang, J., and Lin, Z. (2017a). Meniscus-assisted solution printing of large-grained perovskite films for high-efficiency solar cells. Nat. Commun. *8*, 16045.

He, Y., Du, S., Li, J., Zhang, R., Liang, X., and Chen, B. (2017b). Mesoporous ceria-supported gold catalysts self-assembled from monodispersed ceria nanoparticles and nanocubes: a study of the crystal plane effect for the low-temperature water gas shift reaction. Chemcatchem *9*, 4070–4082.

Hills-Kimball, K., Nagaoka, Y., Cao, C., Chaykovsky, E., and Chen, O. (2017). Synthesis of formamidinium lead halide perovskite nanocrystals through solid–liquid–solid cation exchange. J. Mater. Chem. C *5*, 5680–5684.

Hong, F., Zhang, F., Liu, Y., and Yan, H. (2017). DNA origami: scaffolds for creating higher order structures. Chem. Rev. *117*, 12584–12640.

Jaiswal, J.K., Mattoussi, H., Mauro, J.M., and Simon, S.M. (2003). Long-term multiple color imaging of live cells using quantum dot bioconjugates. Nat. Biotechnol. *21*, 47–51.

Jiang, S., Fang, Y., Li, R., Xiao, H., Crowley, J., Wang, C., White, T.J., Goddard, W.A., Wang, Z., Baikie, T., and Fang, J. (2016). Pressure-dependent polymorphism and band-gap tuning of methylammonium lead iodide perovskite. Angew. Chem. Int. Ed. *55*, 6540–6544.

Kim, J., Kim, H.S., Lee, N., Kim, T., Kim, H., Yu, T., Song, I.C., Moon, W.K., and Hyeon, T. (2008). Multifunctional uniform nanoparticles composed of a magnetite nanocrystal core and a mesoporous silica shell for magnetic resonance and fluorescence imaging and for drug delivery. Angew. Chem. Int. Ed. *47*, 8438–8441.

Kim, J., Lee, J.E., Lee, J., Yu, J.H., Kim, B.C., An, K., Hwang, Y., Shin, C.H., Park, J.G., Kim, J., and Hyeon, T. (2006). Magnetic fluorescent delivery vehicle using uniform mesoporous silica spheres embedded with monodisperse magnetic and semiconductor nanocrystals. J. Am. Chem. Soc. *128*, 688–689.

Kotov, N.A., Dekany, I., and Fendler, J.H. (1995). Layer-by-layer self-assembly of polyelectrolyte-semiconductor nanoparticle composite films. J. Phys. Chem. *99*, 13065–13069.

Kovalenko, M.V., Manna, L., Cabot, A., Hens, Z., Talapin, D.V., Kagan, C.R., Klimov, V.I., Rogach, A.L., Reiss, P., Milliron, D.J., and Guyot-Sionnnest, P. (2015). Prospects of nanoscience with nanocrystals. ACS Nano *9*, 1012–1057.

Ladomenou, K., Natali, M., Iengo, E., Charalampidis, G., Scandola, F., and Coutsolelos, A.G. (2015). Photochemical hydrogen generation with porphyrin-based systems. Coord. Chem. Rev. *304*, 38–54.

Lai, Z., Chen, Y., Tan, C., Zhang, X., and Zhang, H. (2016). Self-assembly of two-dimensional nanosheets into one-dimensional nanostructures. Chem *1*, 59–77.

Lee, N., and Hyeon, T. (2012). Designed synthesis of uniformly sized iron oxide nanoparticles for efficient magnetic resonance imaging contrast agents. Chem. Soc. Rev. *41*, 2575–2589.

Li, F., Lu, J., Kong, X., Hyeon, T., and Ling, D. (2017). Dynamic nanoparticle assemblies for biomedical applications. Adv. Mater. *29*, https://doi.org/10.1002/adma.201605897.

Liao, H.-G., Zherebetskyy, D., Xin, H., Czarnik, C., Ercius, P., Elmlund, H., Pan, M., Wang, L.-W., and Zheng, H. (2014). Facet development during platinum nanocube growth. Science *345*, 916–919.

Lidke, D.S., Nagy, P., Heintzmann, R., Arndt-Jovin, D.J., Post, J.N., Grecco, H.E., Jares-Erijman, E.A., and Jovin, T.M. (2004). Quantum dot ligands provide new insights into erbB/HER receptor-mediated signal transduction. Nat. Biotechnol. *22*, 198–203.

Liong, M., Angelos, S., Choi, E., Patel, K., Stoddart, J.F., and Zink, J.I. (2009a). Mesostructured multifunctional nanoparticles for imaging and drug delivery. J. Mater. Chem. *19*, 6251–6257.

Liong, M., France, B., Bradley, K.A., and Zink, J.I. (2009b). Antimicrobial activity of silver nanocrystals encapsulated in mesoporous silica nanoparticles. Adv. Mater. *21*, 1684–1689.

Liong, M., Lu, J., Kovochich, M., Xia, T., Ruehm, S.G., Nel, A.E., Tamanoi, F., and Zink, J.I. (2008). Multifunctional inorganic nanoparticles for imaging, targeting, and drug delivery. ACS Nano *2*, 889–896.

Liu, W., Halverson, J., Tian, Y., Tkachenko, A.V., and Gang, O. (2016). Self-organized architectures from assorted DNA-framed nanoparticles. Nat. Chem. *8*, 867–873.

Lu, C., and Tang, Z. (2016). Advanced inorganic nanoarchitectures from oriented self-assembly. Adv. Mater. *28*, 1096–1108.

Lu, Z., Ye, M., Li, N., Zhong, W., and Yin, Y. (2010). Self-assembled TiO2 nanocrystal clusters for selective enrichment of intact phosphorylated proteins. Angew. Chem. Int. Ed. *49*, 1862–1866.

Lu, Z., and Yin, Y. (2012). Colloidal nanoparticle clusters: functional materials by design. Chem. Soc. Rev. *41*, 6874–6887.

Luo, D., Qin, X., Song, Q., Qiao, X., Zhang, Z., Xue, Z., Liu, C., Mo, G., and Wang, T. (2017). Ordered superparticles with an enhanced photoelectric effect by sub-nanometer interparticle distance. Adv. Funct. Mater. *27*, 1701982.

Manzeli, S., Ovchinnikov, D., Pasquier, D., Yazyev, O.V., and Kis, A. (2017). 2D transition metal dichalcogenides. Nat. Rev. Mater. *2*, 17033.

Mathew, S., Yella, A., Gao, P., Humphry-Baker, R., Curchod, B.F.E., Ashari-Astani, N., Tavernelli, I., Rothlisberger, U., Nazeeruddin, M.K., and Graetzel, M. (2014). Dye-sensitized solar cells with 13% efficiency achieved through the molecular engineering of porphyrin sensitizers. Nat. Chem. *6*, 242–247.

Mattoussi, H., Palui, G., and Na, H.B. (2012). Luminescent quantum dots as platforms for probing in vitro and in vivo biological processes. Adv. Drug Deliv. Rev. *64*, 138–166.

Medintz, I.L., Uyeda, H.T., Goldman, E.R., and Mattoussi, H. (2005). Quantum dot bioconjugates for imaging, labelling and sensing. Nat. Mater. *4*, 435–446.

Meidan, Y., Chunfeng, H., James, I., Xueqin, L., Xun, C., Xiangtong, M., Matthew, R., Xiaodan, H., Xiangyang, L., and Zhiqun, L. (2017). Recent advances in interfacial engineering of perovskite solar cells. J. Phys. Appl. Phys. *50*, 1–16.

Na, H.B., Lee, J.H., An, K., Park, Y.I., Park, M., Lee, I.S., Nam, D.-H., Kim, S.T., Kim, S.-H., Kim, S.-W., et al. (2007). Development of a T-1 contrast agent for magnetic resonance imaging using MnO nanoparticles. Angew. Chem. Int. Ed. *46*, 5397–5401.

Nagaoka, Y., Hills-Kimball, K., Tan, R., Li, R., Wang, Z., and Chen, O. (2017). Nanocube superlattices of cesium lead bromide perovskites and pressure-induced phase transformations at atomic and mesoscale levels. Adv. Mater. *29*, https://doi.org/10.1002/adma.201606666.

Nam, J., Won, N., Bang, J., Jin, H., Park, J., Jung, S., Jung, S., Park, Y., and Kim, S. (2013). Surface engineering of inorganic nanoparticles for imaging and therapy. Adv. Drug Deliv. Rev. *65*, 622–648.

Ortega, S., Ibanez, M., Liu, Y., Zhang, Y., Kovalenko, M.V., Cadavid, D., and Cabot, A. (2017). Bottom-up engineering of thermoelectric nanomaterials and devices from solution-processed nanoparticle building blocks. Chem. Soc. Rev. *46*, 3510–3528.

Ortgies, D.H., de La Cueva, L., del Rosal, B., Sanz-Rodriguez, F., Fernandez, N., Carmen Iglesias-de la Cruz, M., Salas, G., Cabrera, D., Teran, F.J., Jaque, D., and Martin Rodriguez, E. (2016). In vivo deep tissue fluorescence and magnetic imaging employing hybrid nanostructures. ACS Appl. Mater. Interfaces *8*, 1406–1414.

Pang, X., He, Y., Jung, J., and Lin, Z. (2016). 1D nanocrystals with precisely controlled dimensions, compositions, and architectures. Science *353*, 1268–1272.

Pang, X., Zhao, L., Han, W., Xin, X., and Lin, Z. (2013). A general and robust strategy for the synthesis of nearly monodisperse colloidal nanocrystals. Nat. Nanotechnol. *8*, 426.

Park, J.-E., Hickey, D.R., Jun, S., Kang, S., Hu, X., Chen, X.-J., and Park, S.-J. (2016). Surfactant-assisted emulsion self-assembly of nanoparticles into hollow vesicle-like structures and 2d plates. Adv. Funct. Mater. *26*, 7791–7798.

Park, J., Porter, M.D., and Granger, M.C. (2017). Colloidally assembled zinc ferrite magnetic beads: superparamagnetic labels with high magnetic moments for MR sensors. ACS Appl. Mater. Interfaces *9*, 19569–19577.

Qiu, Y., Chen, P., and Liu, M. (2010). Evolution of various porphyrin nanostructures via an oil/aqueous medium: controlled self-assembly, further organization, and supramolecular chirality. J. Am. Chem. Soc. *132*, 9644–9652.

Quan, Z., Luo, Z., Wang, Y., Xu, H., Wang, C., Wang, Z., and Fang, J. (2013). Pressure-induced

switching between amorphization and crystallization in PbTe nanoparticles. Nano Lett. *13*, 3729–3735.

Quan, Z., Wang, Y., Bae, I.-T., Loc, W.S., Wang, C., Wang, Z., and Fang, J. (2011). Reversal of Hall–Petch effect in structural stability of PbTe nanocrystals and associated variation of phase transformation. Nano Lett. *11*, 5531–5536.

Sanehira, E.M., Marshall, A.R., Christians, J.A., Harvey, S.P., Ciesielski, P.N., Wheeler, L.M., Schulz, P., Lin, L.Y., Beard, M.C., and Luther, J.M. (2017). Enhanced mobility $CsPbI_3$ quantum dot arrays for record-efficiency, high-voltage photovoltaic cells. Sci. Adv. *3*, eaao4204.

Shang, L., Liang, Y., Li, M., Waterhouse, G.I.N., Tang, P., Ma, D., Wu, L.-Z., Tung, C.-H., and Zhang, T. (2017). "Naked" magnetically recyclable mesoporous Au-gamma-Fe2O3 nanocrystal clusters: a highly integrated catalyst system. Adv. Funct. Mater. *27*, 1606215.

Shi, R., Cao, Y., Bao, Y., Zhao, Y., Waterhouse, G.I.N., Fang, Z., Wu, L.-Z., Tung, C.-H., Yin, Y., and Zhang, T. (2017). Self-assembled Au/CdSe nanocrystal clusters for plasmon-mediated photocatalytic hydrogen evolution. Adv. Mater. *29*, https://doi.org/10.1002/adma.201700803.

Suh, W.H., Suh, Y.-H., and Stucky, G.D. (2009). Multifunctional nanosystems at the interface of physical and life sciences. Nano Today *4*, 27–36.

Sun, Y. (2013). Controlled synthesis of colloidal silver nanoparticles in organic solutions: empirical rules for nucleation engineering. Chem. Soc. Rev. *42*, 2497–2511.

Sun, Y., Zuo, X., Sankaranarayanan, S.K.R.S., Peng, S., Narayanan, B., and Kamath, G. (2017). Quantitative 3D evolution of colloidal nanoparticle oxidation in solution. Science *356*, 303–307.

Swarnkar, A., Marshall, A.R., Sanehira, E.M., Chernomordik, B.D., Moore, D.T., Christians, J.A., Chakrabarti, T., and Luther, J.M. (2016). Quantum dot–induced phase stabilization of α-$CsPbI_3$ perovskite for high-efficiency photovoltaics. Science *354*, 92–95.

Taheri Najafabadi, A. (2015). Emerging applications of graphene and its derivatives in carbon capture and conversion: current status and future prospects. Renew. Sustain. Energ. Rev. *41*, 1515–1545.

Tan, R., Zhu, H., Cao, C., and Chen, O. (2016). Multi-component superstructures self-assembled from nanocrystal building blocks. Nanoscale *8*, 9944–9961.

Tang, J., Kemp, K.W., Hoogland, S., Jeong, K.S., Liu, H., Levina, L., Furukawa, M., Wang, X., Debnath, R., Cha, D., et al. (2011). Colloidal-quantum-dot photovoltaics using atomic-ligand passivation. Nat. Mater. *10*, 765–771.

Tao, A.R., Huang, J., and Yang, P. (2008). Langmuir−blodgettry of nanocrystals and nanowires. Acc. Chem. Res. *41*, 1662–1673.

Tian, Y., Zhang, Y., Wang, T., Xin, H.L., Li, H., and Gang, O. (2016). Lattice engineering through nanoparticle-DNA frameworks. Nat. Mater. *15*, 654–661.

Vogel, N., Retsch, M., Fustin, C.-A., del Campo, A., and Jonas, U. (2015). Advances in colloidal assembly: the design of structure and hierarchy in two and three dimensions. Chem. Rev. *115*, 6265–6311.

Wang, D., Hermes, M., Kotni, R., Wu, Y., Tasios, N., Liu, Y., de Nijs, B., van der Wee, E.B., Murray, C.B., Dijkstra, M., and van Blaaderen, A. (2018a). Interplay between spherical confinement and particle shape on the self-assembly of rounded cubes. Nat. Commun. *9*, 2228.

Wang, D., Niu, L., Qiao, Z.-Y., Cheng, D.-B., Wang, J., Zhong, Y., Bai, F., Wang, H., and Fan, H. (2018b). Synthesis of self-assembled porphyrin nanoparticle photosensitizers. ACS Nano *12*, 3796–3803.

Wang, J., Zhong, Y., Wang, L., Zhan, N., Cao, R., Bian, K., Alarid, L., Haddad, R.E., Bai, F., and Fan, H. (2016). Morphology-controlled synthesis and metalation of porphyrin nanoparticles with enhanced photocatalytic performance. Nano Lett. *16*, 6523–6528.

Wang, J., Zhong, Y., Wang, X., Yang, W., Bai, F., Zhang, B., Alarid, L., Bian, K., and Fan, H. (2017). pH-Dependent assembly of porphyrin-silica nanocomposites and their application in targeted photodynamic therapy. Nano Lett. *17*, 6916–6921.

Wang, L., Wang, Y., Dong, S., Deng, Y., and Hao, J. (2018c). Nanocapsules of magnetic Au self-assembly for DNA migration and secondary self-assembly. ACS Appl. Mater. Interfaces *10*, 5348–5357.

Wang, T., Lamontagne, D., Lynch, J., Zhuang, J., and Cao, Y.C. (2013a). Colloidal superparticles from nanoparticle assembly. Chem. Soc. Rev. *42*, 2804–2823.

Wang, T., Li, R., Quan, Z., Loc, W.S., Bassett, W.A., Xu, H., Cao, Y.C., Fang, J., and Wang, Z. (2015). Pressure processing of nanocube assemblies toward harvesting of a metastable PbS phase. Adv. Mater. *27*, 4544–4549.

Wang, T., Wang, X., Lamontagne, D., Wang, Z., and Cao, Y.C. (2013b). Macroscale lateral alignment of semiconductor nanorods into freestanding thin films. J. Am. Chem. Soc. *135*, 6022–6025.

Wang, T., Zhuang, J., Lynch, J., Chen, O., Wang, Z., Wang, X., Lamontagne, D., Wu, H., Wang, Z., and Cao, Y.C. (2012). Self-assembled colloidal superparticles from nanorods. Science *338*, 358–363.

Wright, A., Gabaldon, J., Burckel, D.B., Jiang, Y.B., Tian, Z.R., Liu, J., Brinker, C.J., and Fan, H.Y. (2006). Hierarchically organized nanoparticle mesostructure arrays formed through hydrothermal self-assembly. Chem. Mater. *18*, 3034–3038.

Xue, B., Li, T., Wang, B., Ji, L., Yang, D., and Dong, A. (2018). Self-assembled Fe3O4 nanoparticle-doped TiO2 nanorod superparticles with highly enhanced lithium storage properties. Sustain. Energy Fuels *2*, 616–625.

Yang, K., Fan, H., Malloy, K.J., Brinker, C.J., and Sigmon, T.W. (2005). Optical and electrical properties of self-assembled, ordered gold nanocrystal/silica thin films prepared by sol–gel processing. Thin Solid Films *491*, 38–42.

Yella, A., Lee, H.-W., Tsao, H.N., Yi, C., Chandiran, A.K., Nazeeruddin, M.K., Diau, E.W.-G., Yeh, C.-Y., Zakeeruddin, S.M., and Graetzel, M. (2011). Porphyrin-sensitized solar cells with cobalt (II/III)-based redox electrolyte exceed 12 percent efficiency. Science *334*, 629–634.

Yin, Y., and Alivisatos, A.P. (2004). Colloidal nanocrystal synthesis and the organic–inorganic interface. Nature *437*, 664.

Zang, L., Che, Y., and Moore, J.S. (2008). One-dimensional self-assembly of planar pi-conjugated molecules: adaptable building blocks for organic nanodevices. Acc. Chem. Res. *41*, 1596–1608.

Zhang, N., Wang, L., Wang, H., Cao, R., Wang, J., Bai, F., and Fan, H. (2018). Self-assembled one-dimensional porphyrin nanostructures with enhanced photocatalytic hydrogen generation. Nano Lett. *18*, 560–566.

Zhang, Q., Yin, K., Dong, H., Zhou, Y., Tan, X., Yu, K., Hu, X., Xu, T., Zhu, C., Xia, W., et al. (2017a). Electrically driven cation exchange for in situ fabrication of individual nanostructures. Nat. Commun. *8*, 14889.

Zhang, W., Lai, W., and Cao, R. (2017b). Energy-related small molecule activation reactions: oxygen reduction and hydrogen and oxygen evolution reactions catalyzed by porphyrin- and corrole-based systems. Chem. Rev. *117*, 3717–3797.

Zhang, Y., Lu, F., Yager, K.G., van der Lelie, D., and Gang, O. (2013). A general strategy for the DNA-mediated self-assembly of functional nanoparticles into heterogeneous systems. Nat. Nanotechnol. *8*, 865–872.

Zhao, Y.S., Fu, H., Peng, A., Ma, Y., Liao, Q., and Yao, J. (2010). Construction and optoelectronic properties of organic one-dimensional nanostructures. Acc. Chem. Res. *43*, 409–418.

Zhong, Y., Wang, J., Zhang, R., Wei, W., Wang, H., Lu, X., Bai, F., Wu, H., Haddad, R., and Fan, H. (2014a). Morphology-controlled self-assembly and synthesis of photocatalytic nanocrystals. Nano Lett. *14*, 7175–7179.

Zhong, Y., Wang, Z., Zhang, R., Bai, F., Wu, H., Haddad, R., and Fan, H. (2014b). Interfacial self-assembly driven formation of hierarchically structured nanocrystals with photocatalytic activity. ACS Nano *8*, 827–833.

Zhu, H., Nagaoka, Y., Hills-Kimball, K., Tan, R., Yu, L., Fang, Y., Wang, K., Li, R., Wang, Z., and Chen, O. (2017). Pressure-enabled synthesis of hetero-dimers and hetero-rods through intraparticle coalescence and interparticle fusion of quantum-dot-au satellite nanocrystals. J. Am. Chem. Soc. *139*, 8408–8411.

Zhuang, J., Shaller, A.D., Lynch, J., Wu, H., Chen, O., Li, A.D.Q., and Cao, Y.C. (2009). Cylindrical superparticles from semiconductor nanorods. J. Am. Chem. Soc. *131*, 6084–6085.

Zhuang, J., Wu, H., Yang, Y., and Cao, Y.C. (2007). Supercrystalline colloidal particles from artificial atoms. J. Am. Chem. Soc. *129*, 14166–14167.

Zhuang, J., Wu, H., Yang, Y., and Cao, Y.C. (2008). Controlling colloidal superparticle growth through solvophobic interactions. Angew. Chem. Int. Ed. *47*, 2208–2212.